Clim Dyn (2009) 33:383–408
DOI 10.1007/s00382-008-0468-5

Southern hemisphere winter cold-air mesocyclones: climatic environments and associations with teleconnections

C. Claud · A. M. Carleton · B. Duchiron · P. Terray

Received: 27 February 2008 / Accepted: 3 September 2008 / Published online: 20 September 2008

Abstract Cold-air mesocyclones remain a forecasting challenge in the southern hemisphere middle and higher latitudes, where conventional observations are lacking. One way to improve mesocyclone predictability is to determine their larger-scale circulation environments and associations with teleconnection patterns. To help realize this objective, reanalysis datasets on atmospheric and upper-ocean synoptic variables important in mesocyclone development are composited and compared to previously published mesocyclone spatial inventories. These analyses demonstrate a consistent association between higher frequencies of mesocyclones, greater sea ice extent and large positive differences in the SST minus low-altitude air temperature fields, coinciding with enhanced westerly low-level winds having a southerly component. Composites in the 1979–2001 period also were formed for opposite phases of El Niño Southern Oscillation (ENSO), the Southern Annular Mode (SAM) and the Trans-Polar Index (TPI). Regions likely to be favorable for mesocyclone development relative to climatology were identified. The largest (smallest) variations in meso-cyclogenesis occur in the South Pacific (South Indian Ocean, south of Australia), and are dominated by ENSO. The SAM and TPI are of secondary importance, yet still influential, and exhibit strong regional-scale variations.

Keywords Cold-air mesocyclones · Teleconnections · ENSO · SAM · Composite analysis

C. Claud (✉) · B. Duchiron
Laboratoire de Météorologie Dynamique/IPSL, CNRS, Ecole Polytechnique, Palaiseau, France
e-mail: chclaud@lmd.polytechnique.fr

A. M. Carleton
Department of Geography, Earth and Environmental Systems Institute, Penn State University, University Park, PA 16802, USA

P. Terray
LOCEAN/IPSL, CNRS/IRD/UPMC/MNHN, Paris, France

1 Introduction

Mesoscale cyclonic vortices that develop in cold-air outbreaks, or *cold-air mesocyclones* (Heinemann and Claud 1997), occur frequently in the cold season and transition-season months over middle and higher latitudes of both hemispheres (e.g., Reed 1979; Carleton 1985; Ninomiya 1989; Yarnal and Henderson 1989a, b; Bromwich 1991; Turner et al. 1993; Carleton et al. 1995; Claud et al. 1996; Rasmussen et al. 1996; Rasmussen and Turner 2003). Although they can occur over land (e.g., Mills and Walsh 1988), most mesocyclones develop over the ocean where they tend to be more intense because of the larger vertical fluxes of heat and moisture. Moreover, the cloud structure typically is better developed for oceanic mesocyclones, facilitating their detection on satellite visible and thermal infrared (TIR) images, versus those that develop over snow-covered land, continental ice or ice-shelves (cf. Bromwich et al. 1996). The manual identification of cold-air mesocyclones remains important in meteorological analysis because such systems are not always well represented in numerical weather model output; at least, in their initial stages of development (e.g., Carleton 1995; Carleton et al. 1995; Hewson et al., 2000, Claud et al. 2004). Given that mesocyclones can develop rapidly, and often have associated significant weather (strong winds; heavy precipitation as rain, hail and/or snow; rough seas), they pose a forecasting problem particularly for coastal areas

and shipping interests. Because cold-air mesocyclones tend to develop within favorable larger-scale meteorological environments, especially cold-air advection and positive vorticity (e.g., Harrold and Browning 1969; Mansfield 1974; Rasmussen 1979; Businger and Reed 1989), a useful way to improve the forecast accuracy of these systems is to determine the composite fields of meteorological variables typically associated with their occurrence in different regions and seasons (e.g., Businger 1985, 1987; Fitch and Carleton 1992; Carleton and Fitch 1993; Turner and Thomas 1994; Carleton and Song 1997; Carrasco et al. 1997). These patterns can then comprise "watch areas" for mesocyclone development. Additional explanatory variables for mesocyclone development involve the ocean–atmosphere interaction; primarily, sea surface temperature (SST) and sea-ice conditions at higher latitudes (ice extent, ice concentration), and the temperature in the lowest layers of the atmosphere, as well as its difference from the SST (e.g., Carleton and Carpenter 1989, 1990; Rasmussen et al. 1992; Song and Carleton 1997; Carleton and Song 2000).

Cold-air mesocyclones have a climatic signature in those regions which experience high frequencies of such systems (Lyons 1983; Bromwich 1991; Sinclair and Cong 1992; Turner et al. 1993; Carrasco and Bromwich 1994; Carrasco et al. 2003). For example, Rocky and Braaten (1995) showed that mesocyclones contribute significantly to the annual snowfall at McMurdo station, Antarctica. On decadal and longer time scales it has been speculated (Rasmussen et al. 1993) that mesocyclones may help maintain the higher-latitude branch of the thermo-haline circulation: there is a close spatial correspondence between regions of mesocyclone maxima in the northern North Atlantic and the areas of enhanced downwelling of cold saline water (around Greenland, Labrador). When satellite-image retrieved frequencies and locations of mesocyclones are aggregated on monthly and seasonal time scales (e.g., as mapped distributions; tabulated zonal totals or averages), they reveal associations with the large-scale atmospheric circulation and teleconnection patterns, such as the El Niño Southern Oscillation (ENSO) (Carleton and Carpenter 1990; Carleton and Song 1997, 2000) and the North Atlantic Oscillation (NAO) (Carleton 1985; Harold et al. 1999, Claud et al. 2007). In general, increased monthly and seasonal frequencies of cold-air mesocyclones occur in areas having amplified anomalies in the 500 hPa height field over middle and higher latitudes; either within the anomalous trough or between the trough and the upstream ridge (i.e., the region of persistent cold advection) (Businger 1987; Ese et al. 1988; Fitch and Carleton 1992; Carleton and Fitch 1993; Turner and Thomas 1994; Carleton and Song 1997). The probability of large numbers of mesocyclones increases where and when these conditions coincide with positive anomalies of the SST-near-surface air temperature difference and more extensive sea ice, such as the north-west North Pacific, the Labrador and East Greenland seas, the Barents Sea, and the Ross and Bellingshausen/Amundsen seas (Antarctica) (e.g., Yarnal and Henderson 1989a; Ninomiya 1989; Carleton and Carpenter 1990; Rasmussen et al. 1992, 1996; Moore et al. 1996; Carleton and Song 1997). Thus, it should be possible to improve the predictability of cold-air mesocyclone susceptible areas on monthly to seasonal time scales, from determination of the typical associations between mesocyclone-favored environments (atmospheric, oceanic, sea ice) and larger-scale circulation teleconnections.

The southern hemisphere (SH) extratropics (Fig. 1) comprise a highly worthwhile candidate for undertaking a climatic analysis of cold-air mesocyclone environments and their larger-scale associations, for the following reasons: (1) The middle latitudes are dominated by ocean, over which mesocyclones occur with considerable frequency (Streten and Troup 1973; Carleton 1979); (2) New Zealand and coastal areas of western South America, southern Australia, and South Africa are affected by mesocyclones in the colder season (e.g., Carleton 1981), when these systems form over higher-middle latitudes and move north-eastward in the cold-air outbreaks behind major frontal cyclones; (3) The Antarctic sea ice undergoes large annual and interannual variations in extent and concentration, especially regionally (e.g., Zwally et al. 1979; Carleton and Carpenter 1989; Carleton and Fitch 1993; Yuan et al. 1999; Yuan and Martinson 2000); (4) Important large-scale climatic

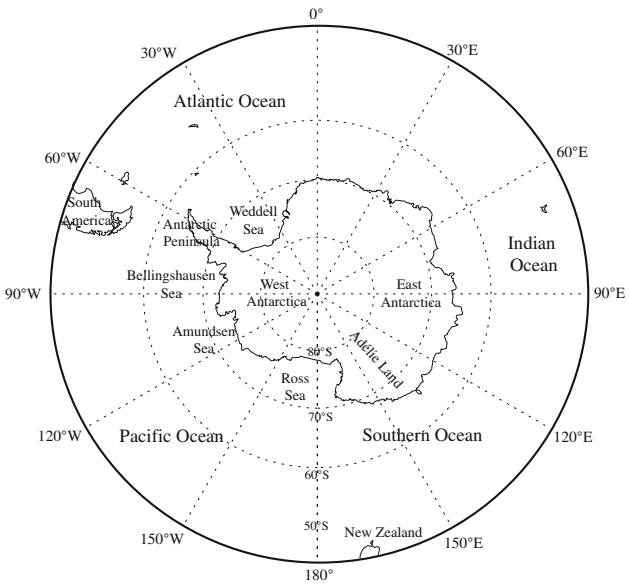

Fig. 1 Map of Antarctica, indicating geographic features mentioned in the text

teleconnections -especially ENSO- either originate or have centers of action in the SH that influence higher latitudes, such as the Pacific South America (PSA) pattern (e.g., Mo and Ghil 1987; Farrara et al. 1989; Carleton 1988, 1989, 2003; Carleton and Carpenter 1990; Turner 2004; Fogt and Bromwich 2006); (5) Large departures from the time-averaged zonal circulation can occur on monthly and seasonal time scales, evident as meridionally-varying pressure/height anomaly patterns and associated climate anomalies (Streten 1977; Harangozo 1997); and (6) Several studies have determined the spatial distributions of mesocyclone cloud vortices on monthly and seasonal time scales for a number of years representative of large-scale circulation anomalies, from the analysis of TIR images acquired by polar-orbiting satellites (Carleton and Carpenter 1990; Carleton and Fitch 1993; Carleton and Song 1997). At the time those studies (i.e., 6) were conducted, datasets on atmospheric and oceanic variables were less comprehensive than they are now. Thus, those mapped analyses of mesocyclones can be independently compared with the high quality "long-term" reanalyses newly available, to better characterize mesocyclone typical environments for winter, and their associations (statistical, visual) with larger-scale circulation patterns and teleconnections identified. These are the objectives of the present paper.

The paper is organized as follows. In the next section, the data and methods are presented. In Sect. 3, we identify the variables most pertinent to describing areas having high densities of cold-air mesocyclones, based on comparisons between previously-published inventories of mesocyclones and reanalysis fields. Then, following presentation of the large-scale teleconnection modes and their statistical interrelationships, we describe associations between the mesocyclone-significant variables and the large-scale circulation; the latter given by temporal inter-correlations of teleconnection indices and spatial composites of mesocyclone variables. From those composite results, we identify the spatial areas likely to see enhanced and also suppressed, meso-cyclogenesis relative to background levels—the meso-cyclogenesis potential—for comparison with previously published mesocyclone inventories. In Sect. 4, the results of the study are summarized and discussed.

2 Data and analysis

Fulfillment of the above objectives utilizes both conventional, satellite-based, and merged/combined datasets on atmospheric, oceanic and sea ice variables pertinent to SH mesocyclone occurrence and its spatial distribution, on monthly and seasonal to interannual time scales. Stratified composite analysis is applied to these datasets.

2.1 Satellite TIR images for mesocyclone identification

To justify our choice of meteorological variables used to depict the environments within which cold-air mesocyclones develop (Sect. 3.2); to help demonstrate their associations with SH teleconnections (Sect. 3.3 and 3.4); and to provide verification for the maps of meso-cyclogenesis potential derived from the reanalysis composites (Sect. 3.5), we compare (Sect. 3.1) monthly and seasonal averages of the mapped fields with (1) the hemispheric distributions of polar lows identified for the contrasting winter seasons (JJAS) of 1979, 1981 and 1982, depicted in Carleton and Carpenter (1990; hereafter CC90); and (2) for the individual June–July–August months of 1988 and 1989 centered on the "half-hemisphere" between approximate longitudes 100°E eastward to 50°W (Carleton and Fitch 1993; hereafter CF93). The winter seasons and months studied represent large variations in the climate system of the SH, including El Niño events of different intensity (1982, 1988) and a strong La Niña (1989). More specifically, winter 1988 and 1989 depict the rapid change from El Niño to La Niña-dominated circulation regimes (CF93, their Fig. 8; Cullather et al. 1996). Winter seasons 1981 and 1982 comprised, respectively, the year preceding (i.e., year-1) and the year of (year0) the major El Niño event of 1982–1983. Winter 1979 was characterized by an anomalously vigorous broader-scale westerly circulation that resembled a combination of El Niño and La Niña events, depending on latitude zone considered (Guymer and LeMarshall 1980; van Loon and Rogers, 1981): it coincided with the first GARP (Global Atmospheric Research Program) global experiment (FGGE) year.

In the CC90 study, mesocyclones were identified from the interpretation of twice-daily TIR images on a polar stereographic projection for the SH, and which comprised the Defense Meteorological Satellite Program (DMSP) dataset. Pattern recognition (i.e., visual assessment) of cloud vortex signatures was employed to find mesocyclones, and classify them either as "inverted comma" single-band system (i.e., comma cloud) or multi-band system (spiraliform) types (Forbes and Lottes 1985; Carleton and Carpenter 1989; Heinemann 1990; Turner et al. 1993; Carleton 1995; McMurdie et al. 1997). The comma cloud vortices typically represent deep baroclinity and occur in cold advection within the larger circulation of frontal cyclones (e.g., Mansfield 1974; Reed 1979; Carleton 1987; Businger and Reed 1989); the spiraliform type tends to occur at higher latitudes deep within cold-air (i.e., more barotropic conditions: Rasmussen 1979, 1981; Rasmussen et al. 1992; Turner et al. 1993). The mesocyclone information was depicted in map format for each winter season and month considered (Figs. 2, 3). For these latitudes, the polar-orbiting DMSP is advantageous for

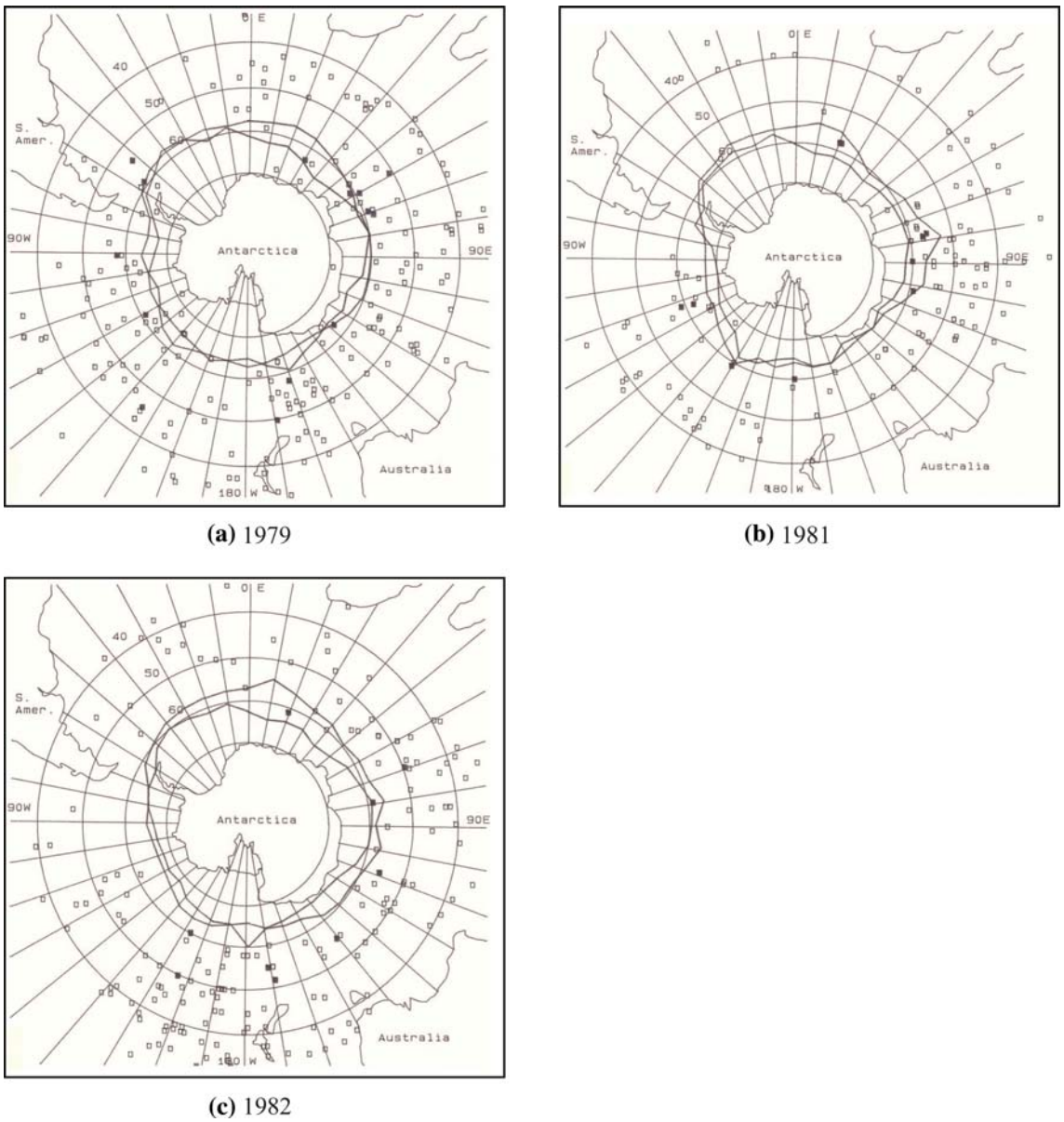

Fig. 2 Locations of winter-season (June–September) mesocyclones for **a** 1979, **b** 1981, **c** 1982. Comma clouds are shown as *open squares*, spiraliform systems are shown as *filled squares* (see text for details). The June and September sea ice extents are also shown (from CC90)

studying mesocyclone occurrences compared, for example, to geosynchronous satellite data (cf. Carleton and Song 1997). Two IR composite images per day were generated for the hemisphere, and the nominal 0.6 km^2 resolution of the DMSP was reduced to 5.4 km^2 for the purpose of showing the synoptic-scale context of cloud fields and cloud systems. The coarser resolution is unlikely to have affected the detection of mesocyclones to any appreciable extent because shorter-lived systems also tend to be weaker, and most mesocyclones are readily detected at 5.4 km^2 resolution (e.g., Carleton 1987). Further discussion on the DMSP imagery used to derive mesocyclone climatologies is given in CC90 and CF93.

2.2 Long-term high resolution reanalyses

Large-scale reanalysis fields are derived from the ERA-40 data assimilation system, which uses the integrated forecasting system (IFS) developed jointly by ECMWF and Météo-France (Simmons and Gibson 2000). A three-dimensional variational method assimilates observations into the spectral model, which has 60 vertical levels and T159 horizontal spectral resolution. Data are available since 1957 for 23 pressure levels with a spatial resolution of 1.125° (approximately 125 km). However, because ERA-40 data have significant shortcomings in high southern latitudes before 1979 and the advent of

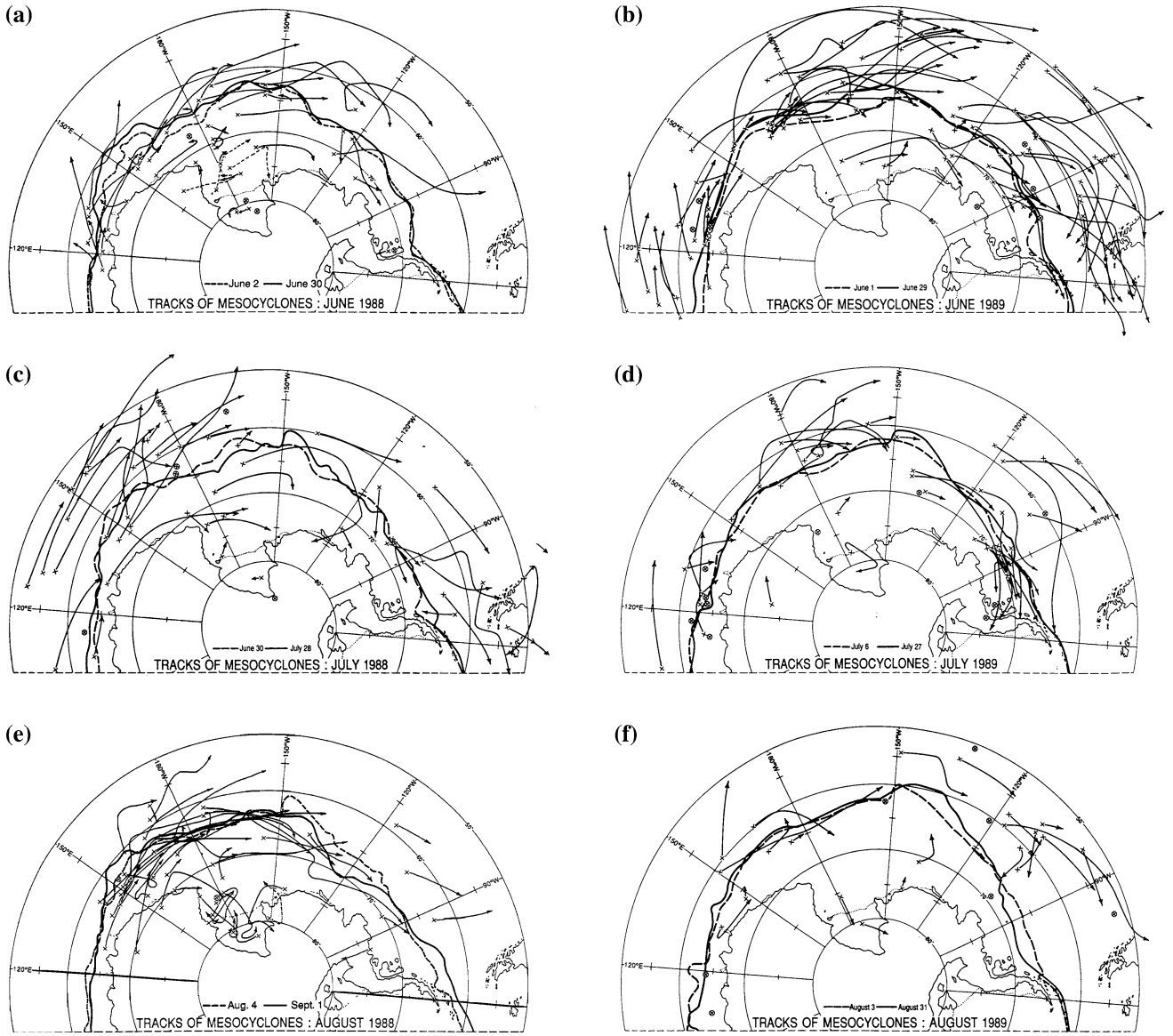

Fig. 3 Mesocyclone trajectories (start and end points, tracks) for **a** June 1988, **b** June 1989, **c** July 1988, **d** July 1989, **e** August 1988, **f** August 1989 (from CF93)

operational satellite retrievals (e.g., Bromwich and Fogt 2004; Sterl 2004), the results utilizing ERA-40 that are presented here cover the period 1979–2001. A more detailed description of the ERA-40 dataset can be obtained online at http://www.ecmwf.int/research/era.

Although SST are available in ERA-40, we utilize the Extended Reconstructed SST (ERSST), which corresponds to a monthly extended reconstruction of global SST based on the comprehensive ocean–atmosphere data set. In ERSST, sea ice concentrations improve the high-latitude SST analysis as the data have undergone stringent quality control (Smith and Reynolds 2003, 2004). SSTs are available on a 2° spatial grid at the following address: http://lwf.ncdc.noaa.gov/oa/climate/research/sst/sst.html#ersst.

Sea ice concentrations are taken from http://nsidc.org/data/seaice_index/; they are retrieved from NIMBUS-7 SSMR and DMSP SSM/I passive microwave radiances (Cavalieri et al., 1996). We regridded the sea ice data onto the ERA-40 grid.

2.3 Statistical analysis

To characterize the associations between low-frequency (climatic) circulation and mesocyclones, we perform temporal inter-correlations of teleconnection indices and derive spatial composites of the atmospheric fields. The monthly indices were acquired from: http://www.cdc.ncep.noaa.gov/. For ENSO, because the peak in most indices

typically occurs in the SH summer, we have considered a seasonal index calculated by averaging the Nino 3.4 index over the broad seasonal period October through February. The statistical significance of the mapped results are assessed using a phase-scrambling bootstrap test with 999 samples (Davison and Hinkley 1997), taking into account the autocorrelation characteristics of each time series analyzed.

3 Results

3.1 Associations of mesocyclone spatial distributions with reanalysis fields

The hemispheric to regional-scale mapped distributions of mesocyclones for sample winter seasons (1979, 1981, 1982) and months (June–July–August 1988 and 1989) representative of a range of circulation anomaly patterns including ENSO, are compared with the reanalysis fields of variables considered to depict mesocyclone-associated atmospheric environments. Because many polar mesocyclones are triggered by upper-level cold troughs, the temperature and the geopotential height at 500 hPa are considered (e.g., Carleton and Fitch 1993; Turner and Thomas 1994). The SST is a critical variable for at least two reasons: first, mesocyclones often form at and just equatorward of the sea ice margin, in connection with pre-existing shallow boundary-layer fronts; second, because of the importance of surface-atmosphere thermodynamical fluxes for their intensification**.** A number of modeling studies have shown that without the contribution of the latter, mesocyclones would not develop beyond the stage of a moderately strong trough (e.g., Emanuel and Rotunno, 1989; Claud et al. 2004). In addition, the difference between the SST and the temperature at 925 hPa is an indicator of the static stability (i.e., we infer the sign and relative magnitude of the surface-atmosphere heat fluxes), such that strongly positive values indicate instability and convection from the surface. Surface heat flux values are not explicitly considered here; instead, winds at 925 hPa are used: enhanced winds imply increased fluxes, and in addition, they provide information on the mean flow direction.

In winter 1979, mesocyclones were frequent and occurred over most of the SH middle and higher latitudes with little longitudinal differentiation evident (Fig. 2a), in association with the anomalously strong westerly circulation. In accord with the change in the annual cycle of the Tasman Sea trough that typically accompanies the evolution of an El Niño event (e.g., van Loon, 1984); from suppressed in year-1 (here, 1981) to enhanced in year0 (1982), the longitudes of maximum frequency of mesocyclones shifted from the southern Indian Ocean to the region around New Zealand between these 2 winters (Fig. 2b, c). The individual winter month maps of 1988 and 1989 reveal large differences in mesocyclone activity (system locations, tracks) between the Ross and Bellingshausen/Amundsen sea sectors (Fig. 3), representative of the change from El Niño to La Niña regimes. Specifically, in winter 1988, mesocyclone activity occurred frequently off the Adelie Land coast eastward through the Ross Sea sector, while there was a lack of such activity eastward of about 135°W; in the Amundsen and Bellingshausen seas (Fig. 3a). In winter 1989 (e.g., Fig. 3b), by contrast, most mesocyclone activity occurred further east, especially in the Amundsen/Bellingshausen sector. These changes in most frequent mesocyclone activity between winters 1988 and 1989 accompanied a reversal of the sea-level pressure anomaly pattern across the "half hemisphere" 120°E through 180° to 60°W, and a corresponding eastward shift in the longitudes of frequent cold-air advection (CF93, their Fig. 8).

As shown in the CC90 and CF93 studies, the spatial frequency variations of mesocyclone activity over higher southern latitudes were accompanied by large regional and longitude sector anomalies of the Antarctic sea-ice extent (i.e., latitude location of the ice edge). On weekly through interannual time scales, the mesocyclone-sea ice edge winter relationship consistently was as follows: greater (reduced) ice extent and more (fewer) mesocyclones in that longitude zone and also somewhat to the eastward (westward). This relationship involves thermal advection by the low-level winds: cold (warm) advection assists ice growth and advance (ice retreat or stagnation), as documented by a number of authors (e.g., Budd 1975; Weatherly et al. 1991; CF93; Carleton 1989; Yuan et al. 1999; Carleton and Song 2000). The availability of digital datasets on Antarctic sea-ice extent and concentration (Sect. 2.2) and the ERA reanalyses permits us to elaborate upon the associations between sea ice conditions, atmospheric variables and mesocyclone distributions over higher southern latitudes, for the winter months and seasons studied in CC90 and CF93. As examples, the September minus June sea ice conditions (extent, concentration) and superimposed mean T500 fields for August 1988 and 1989 (Fig. 4a, b), confirm (cf. Streten and Pike 1980; Cavalieri and Parkinson 1981) that longitudes seeing greater ice extent, and strong ice advance during winter accompany thermal troughs. Conversely, longitude sectors having a stagnant ice edge or one that retreats on these time scales typically are accompanied by thermal ridges. The equivalent barotropic character of the SH extratropical circulation when averaged monthly (e.g., van Loon 1980) means that height troughs (ridges) coincide with longitude sectors of greater (reduced) ice extent; therefore, the mid-tropospheric temperature or

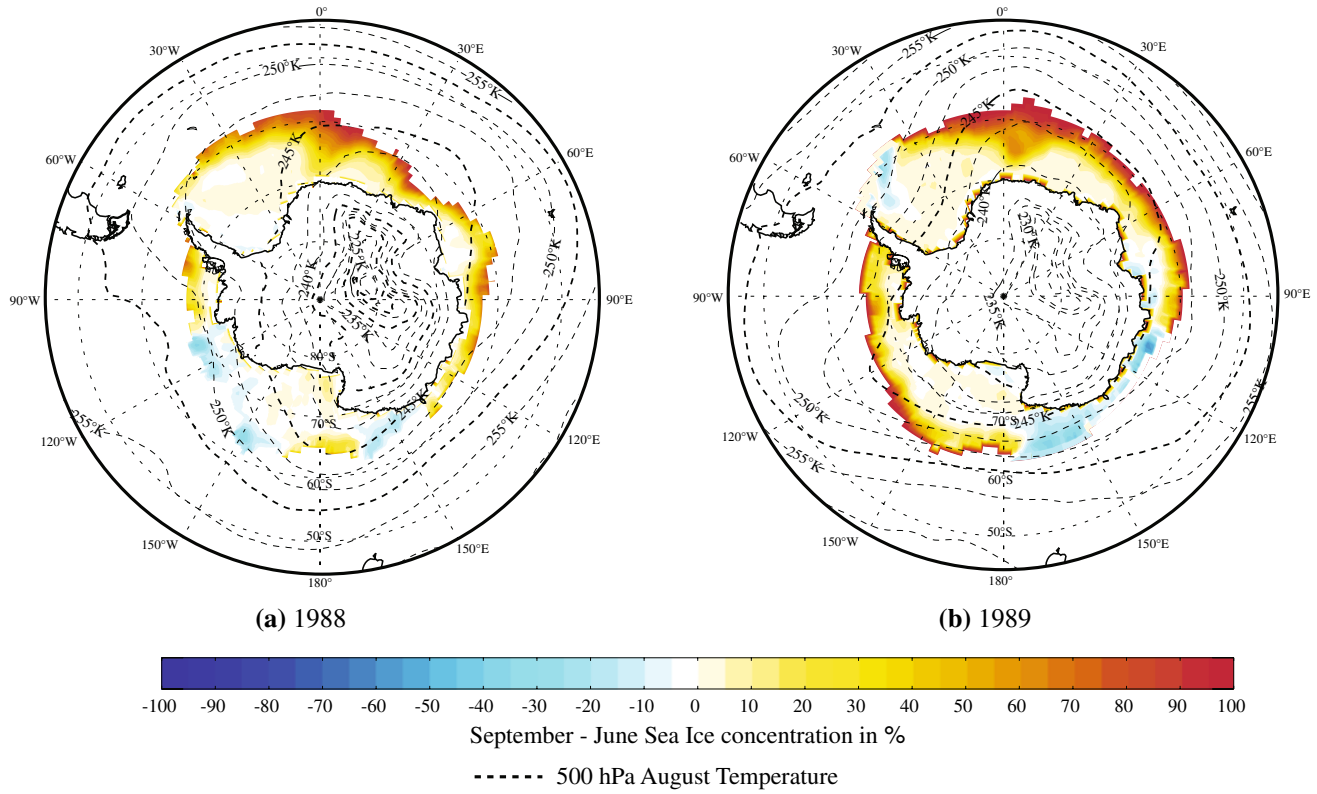

Fig. 4 Sea ice concentration differences between September and June (in %), and temperatures at 500 hPa (T500, K) in August for **a** 1988, **b** 1989

thickness pattern can substitute for the height field on climatic time scales, and provide additional information on teleconnections (cf. Smith and Stearns 1993). Moreover, identification of the relationships between SH mesocyclone activity and variables representing the free-atmosphere circulation and surface-atmosphere forcing, can utilize both low-altitude and mid-tropospheric pressure levels represented in the reanalysis datasets; at least, for first examination.

In the three case study winters for which mesocyclone data are recorded for the full SH extratropics (i.e., 1979, 1981, 1982; CC90), a consistent spatial association is observed (Fig. 5) between higher densities of cold-air mesocyclones and large positive differences in the SST-T925 field that coincide with enhanced low-level westerly winds (i.e., V925), especially where the latter have a southerly component. Such an association is reasonable physically given that comma clouds in particular are favored where increased surface-atmosphere fluxes of heat and moisture occur; west of large synoptic-scale cyclones, in the sector of strongest cold advection. In winter 1979 (Fig. 5a; also Streten 1983), these conditions occurred over most of the SH extratropics, with the exception of around longitude 140°E between about 50°–60°S (weaker positive differences and **V**925 having northerly components). Interestingly, very few mesocyclones were observed in this area (Fig. 2b) contrasted with much of the hemisphere. The unfavorable conditions are likely also related to this region being upstream of a 500 hPa trough, and under generally northerly flow from the associated cyclonic circulation (Streten and Pike 1980).

The high frequencies of mesocyclones in the southern Indian Ocean for winter 1981 (i.e., El Niño year-1) correspond both to extensive sea-ice conditions (Fig. 5b) and large ocean to air fluxes of heat and moisture. The latter are inferred from the larger southerly component of **V**925 winds that blow over increasingly positive differences of SST-T925 in these longitudes (Fig. 5b). Conversely, the dearth of mesocyclones in longitudes of eastern Australia, the Tasman Sea and New Zealand in winter 1981, again coincides with the presence of only small differences in SST-T925 and with **V**925 having a dominantly northerly component. The latter feature expresses the weakened Tasman Sea trough characteristic of El Niño year-1 (van Loon 1984). An eastward shift in the areas of most frequent mesocyclone activity to the Tasman Sea-New Zealand sector for winter 1982 (i.e., El Niño year0), occurs in association with the larger SST-T925 vertical differences and enhanced longitudinal gradients, along with considerably stronger **V**925 and greater sea ice, than

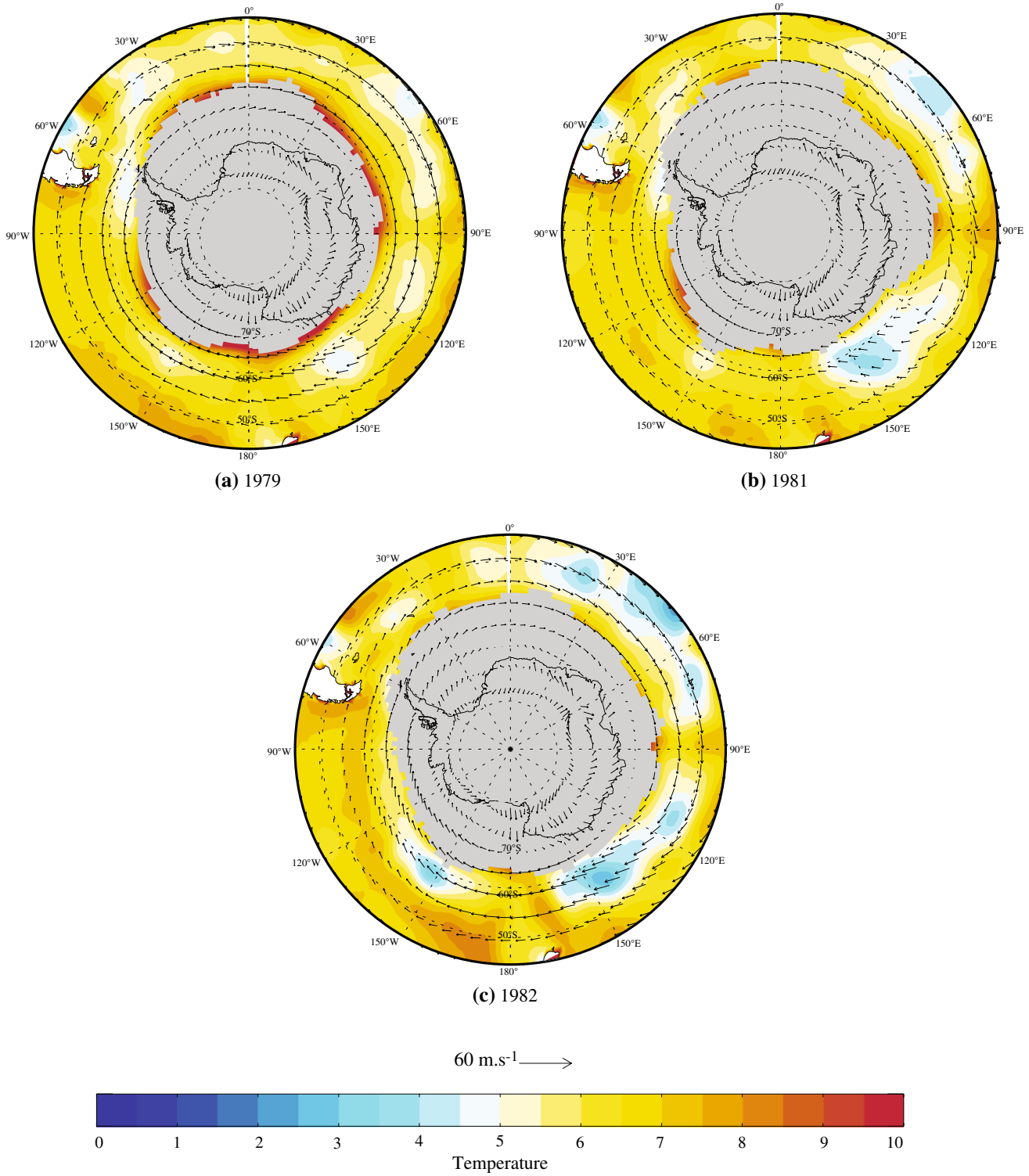

(a) 1979 **(b)** 1981

(c) 1982

Fig. 5 Averaged JJAS wind at 925 hPa (**V**925, m/s) and difference between SST and temperature at 925 hPa (T925, K) for **a** 1979, **b** 1981, **c** 1982. *Gray areas* correspond to grid points where at least one SST monthly value used to construct the average was set as "undefined" because of the presence of land or sea ice

occurred here in 1981 (Fig. 5c). In the southern Indian Ocean for winter 1982, contrasted with the situation there in 1981, sea ice is less extensive; the SST-T925 difference is smaller; and low-altitude winds have a reduced southerly component. These less favorable conditions for mesocyclone development likely explain the

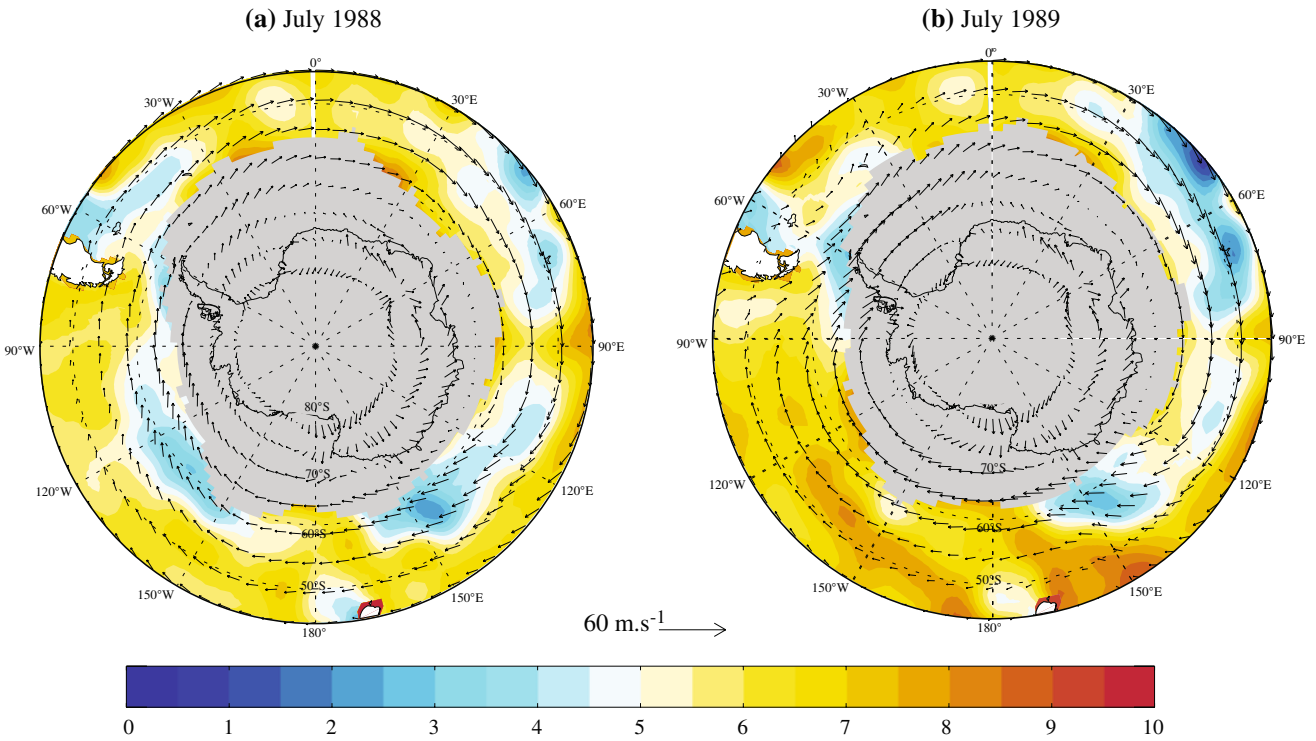

Fig. 6 Wind at 925 hPa (**V**925, m/s) and difference between SST and air temperature at 925 hPa (T925, K) for **a** July 1988, **b** July 1989. *Gray areas* correspond to grid points where the SST was set as "undefined" because of land or sea ice

reduced frequencies of mesocyclones observed in this region for winter 1982.

Examining the fields of SST-T925 and **V**925 for the two July months of 1988 and 1989 (Fig. 6a, b), supports the generalized relationships with cold-air mesocyclone activity noted above for the other winters: mesocyclone frequencies tend to increase in those longitudes characterized by more sea ice (greater extent, higher ice-water concentration), and where stronger westerlies have a component that is more southerly than northerly, blowing over increasingly positive differences of sea-air temperature (e.g., the Ross Sea sector in both winters of 1988 and 1989; much of the Amundsen/Bellingshausen sector in winter 1989). Conversely, the lack of mesocyclones in the latter sector in winter 1988 (Fig. 3a) can be explained by northerly winds blowing over only weakly positive differences of SST-T925 (Fig. 6a).

3.2 Teleconnections and their inter-relationships

The principal mode of atmospheric variability of the extratropical regions of the SH, the so-called SAM (Southern Annular Mode), has a zonally and symmetric (annular) structure (e.g., Kidson 1999; Limpasuvan and Hartmann 1999; Thompson and Wallace 2000; Carleton 2003). The equivalent barotropy reflects the fact that the SAM is driven by anomalies in the eddy flux of zonal momentum at middle latitudes, such that during its positive (negative) phase, the anomalous poleward flux of eddy momentum drives westerly (easterly) anomalies at 55–60°S (e.g., Karoly 1990; Limpasuvan and Hartmann 2000). In recent years, for reasons still debated, the SAM has shifted into its positive phase, denoted by a decrease in surface pressure over the Antarctic and a strengthening of the westerlies in the coastal region as pressure has risen over middle latitudes (e.g., Gong and Wang 1999; Renwick 2004).

The El Niño Southern Oscillation (ENSO) is the dominant global-scale mode of interannual climate variability. While its origin lies in sea-air interactions over tropical regions, it also affects higher southern latitudes via atmospheric teleconnections (e.g., PSA). Turner (2004) reviews how the ENSO signal might be transmitted from the tropical Pacific to the Antarctic, and examines the evidence for such signatures in, among other data, the Antarctic station meteorological records. The most pronounced signal of ENSO occurs over the southeast Pacific as a result of a Rossby wave train that gives positive (negative) height anomalies over the Amundsen-Bellingshausen Sea during warm (cold) events, and the reverse pattern in the Weddell Sea. This high latitude component of the PSA pattern comprises the regional-scale Antarctic dipole index (ADP) developed by Yuan and Martinson (2000, 2001) to capture the out-of-phase variations of the Amundsen and Weddell Sea lows represented in the SLP, surface temperature and

sea ice fields (cf. Carleton 1988). However, relationships with ENSO might not be stable with time (Carleton 1989; Bromwich et al. 2000), and recent papers have discussed possible inter-decadal variability of ENSO teleconnections to the high latitude South Pacific in relationship with the SAM (e.g., Fogt and Bromwich 2006; L'Heureux and Thompson 2006). According to the latter authors, this interdecadal variability is prominent during austral summer, and became amplified in the 1990s during austral spring.

In addition to ENSO and SAM, zonally asymmetric teleconnections that are essentially extratropical in origin show important associations with temperature, meridional wind and precipitation for key sectors of the Southern Ocean, the first two variables being connected to Antarctic sea ice anomalies (Harangozo 1997). In particular, the Trans-Polar Index (TPI)—defined as the SLP anomaly difference between Hobart and Stanley (Pittock 1980, 1984; Rogers and van Loon 1982; Carleton, 1989, 2003)—depicts the eccentricity of wavenumber one. In its positive (negative) phase, TPI expresses an enhanced ridge (trough) in the Australian region and an enhanced trough (ridge) in the South American Sector. A possible lagged positive association between ENSO and TPI that is dependent on time period considered, has been noted by Pittock (1984) and Carleton (1989, 2003).

Before establishing associations between the large-scale teleconnections and atmospheric variables pertinent to mesocyclones, and in view of the sometimes contradictory results obtained by other authors, we present updated inter-correlations between the teleconnection indices (SAM, ENSO, TPI) and discuss these below. The stability of the correlations is assessed by calculation for the period studied here ("recent"; 1979–2001), and also for the preceding period 1957–1978. Only correlations for winter months (June–September), presented in Table 1, are discussed. Correlations with SAM and TPI at ENSO year-1 and year0 have been determined.

It is evident (Table 1) that the TPI and SAM are significantly correlated towards the end of SH winter. Correlation coefficients are positive and the correlations

Table 1 Correlation coefficients between teleconnection indices for winter months (June through September) and over different time periods

	1957–1978				1979–2001			
TPI	SAM							
	June	July	August	September	June	July	August	September
June	0.28	−0.21	0.17	**0.31**	0.23	−0.32	0.06	0.24
July	0.26	**0.38**	**0.33**	0.23	0.12	0.21	**0.62**	0.34
August	−0.05	0.16	**0.32**	0.26	−0.02	0.34	**0.51**	0.21
September	−0.06	0.10	**0.42**	**0.47**	−0.19	0.09	**0.65**	**0.67**

	$NINO_{year0}$	1957–1978	1979–2001	1979–1990	1991–2001
SAM	June	0.10	−0.05	−0.17	0.11
	July	−0.16	−0.10	−0.04	−0.15
	August	**0.37**	0.22	0.08	0.35
	September	0.20	0.08	−0.39	0.46
TPI	June	0.08	0.05	0.21	−0.16
	July	**−0.35**	**0.48**	**0.75**	0.26
	August	0.14	0.17	0.17	0.17
	September	−0.03	0.04	−0.20	0.19
	$NINO_{year-1}$	1957–1978	1979–2001	1979–1990	1991–2001
SAM	June	−0.17	0.30	0.41	0.19
	July	0.01	−0.04	−0.17	0.06
	August	**−0.42**	0.30	**0.65**	−0.03
	September	−0.29	0.20	**0.59**	−0.13
TPI	June	**0.35**	0.26	0.36	0.14
	July	**0.39**	0.17	0.28	0.08
	August	−0.06	−0.18	0.34	**−0.52**
	September	0.10	0.30	0.45	0.21

Values in bold are significant at the 90% level

are larger for the recent period than for the preceding period, for which TPI was also correlated with the SAM in July.

The ENSO at year 0 is positively correlated with SAM in August, with significant values for the preceding period ($r = 0.37$) but not for the recent period ($r = 0.22$). At year-1 for the recent period, SAM and ENSO are slightly positively correlated, but never significant at the 90% level. However, for the preceding period, SAM and ENSO were anti-correlated, with larger values in August ($r = -0.42$; significant at the 90% level).

At year0, TPI and ENSO are only significantly correlated in July. The sign changes from negative to positive between the two periods. At year-1, TPI and ENSO are positively correlated in June–July (significant during the preceding period; not significant during the recent period). The significance in the preceding period confirms results by Pittock (1984) and Carleton (1989), who found that TPI leads ENSO by up to one year. However, the result for the recent period confirms that this association is not stable over multiple decades.

Because of the changes observed between the two periods (1957–1978; 1979–2001), and given that a growing number of studies show an apparent reversal in statistical correlations between ENSO and Antarctic-region climate (e.g., precipitation: Genthon and Cosme 2003; Fogt and Bromwich 2006; Thomas et al. 2008), we decided to check whether the correlations were consistent within the recent period. Accordingly, correlations have been calculated separately for 1979–1990 (i.e., first subset of the recent period) and 1991–2000 (second subset).

At year0 (Table 1), SAM and ENSO are never significantly correlated, but the sign of the correlations in June and September changes from the first subset to the second. At year-1, SAM and ENSO are positively correlated in August ($r = 0.65$) and September ($r = 0.59$) for sub-period 1979–1990, but not for sub-period 1991–2000 (when correlations become negative but non-significant at the 90% level).

For ENSO and TPI at year0, correlations are significant in July for the first subset of the recent period ($r = 0.75$) but not in the second subset**.** The sign of the correlations in both June and September changes from the first subset to the second. At year-1, correlations are positive but never significant for sub-period 1979–1990, yet become lower and even negative in August of sub-period 1991–2000 ($r = -0.52$; significant at the 90% level).

The correlations between indices representing the dominant SH low-frequency circulation patterns, support previous findings showing that the ENSO teleconnection to higher southern latitudes is not consistent over time (e.g., Bromwich et al. 2000). On the other hand, they show that for the period of interest in our study (1979–2001), the derivation of spatial composites of reanalysis variables is justified because of the independence of the major teleconnections (ENSO, SAM, TPI) in most months. Because SAM and TPI are significantly correlated in late winter, they will be discussed together.

3.3 Composite patterns of reanalysis fields associated with teleconnections

Having established the value of depicting SH winter mesocyclone favored regimes from reanalysis fields of SST-T925 and **V**925 (Sect. 3.1), we present the composite anomaly maps of those variables for extreme phases of the dominant teleconnection indices ENSO, SAM and TPI (1979–2001). The geostrophic approximation permits one to infer the anomalies of near-surface atmospheric pressure from the spatial patterns of **V**925. We discuss only those areas having statistical significance larger than 90%. Because the significances are computed with respect to the composite mean expressed as a departure from the mean, they are relatively conservative compared to what would be expected when computing significances of the differences between opposite extremes in the indices.

The winter early (June) and late (September) months comprise opposite phases of the Semi-Annual Oscillation (SAO) of pressure/height that maximizes over sub-antarctic and Antarctic latitudes (e.g., van Loon 1967; van Loon and Rogers 1984). Because the SAO is expressed as a latitude shift in the circumpolar trough, such that it is displaced equatorward of its annual mean position in June, and poleward in September, its location directly influences the low-level winds (westerlies to the north; easterlies to the south): on average, there is an inter-seasonal change in the strength and direction of the winds near the Antarctic coast. Indeed, these inter-seasonal reversals in the winds are involved in the annual pattern of sea-ice growth and retreat, via their influences on temperature advection and the ice convergence and divergence (Enomoto and Ohmura 1990; Lefebvre and Goosse 2008). Given the importance of SAO, we show the composites for both June and September months, representing early and late winter conditions respectively, and compare the patterns for similar months across different phases of the teleconnections.

3.3.1 ENSO

Composite anomaly fields of SST-T925 and **V**925 in winters ENSO year-1 and year0 are displayed for June and September on Fig. 7. As explained above, Fig. 7 shows significant changes during the season. For example, the extensive areas of strongly positive vertical temperature difference anomalies in June shrink and change to negative by September (e.g., the Indian Ocean). As shown for the

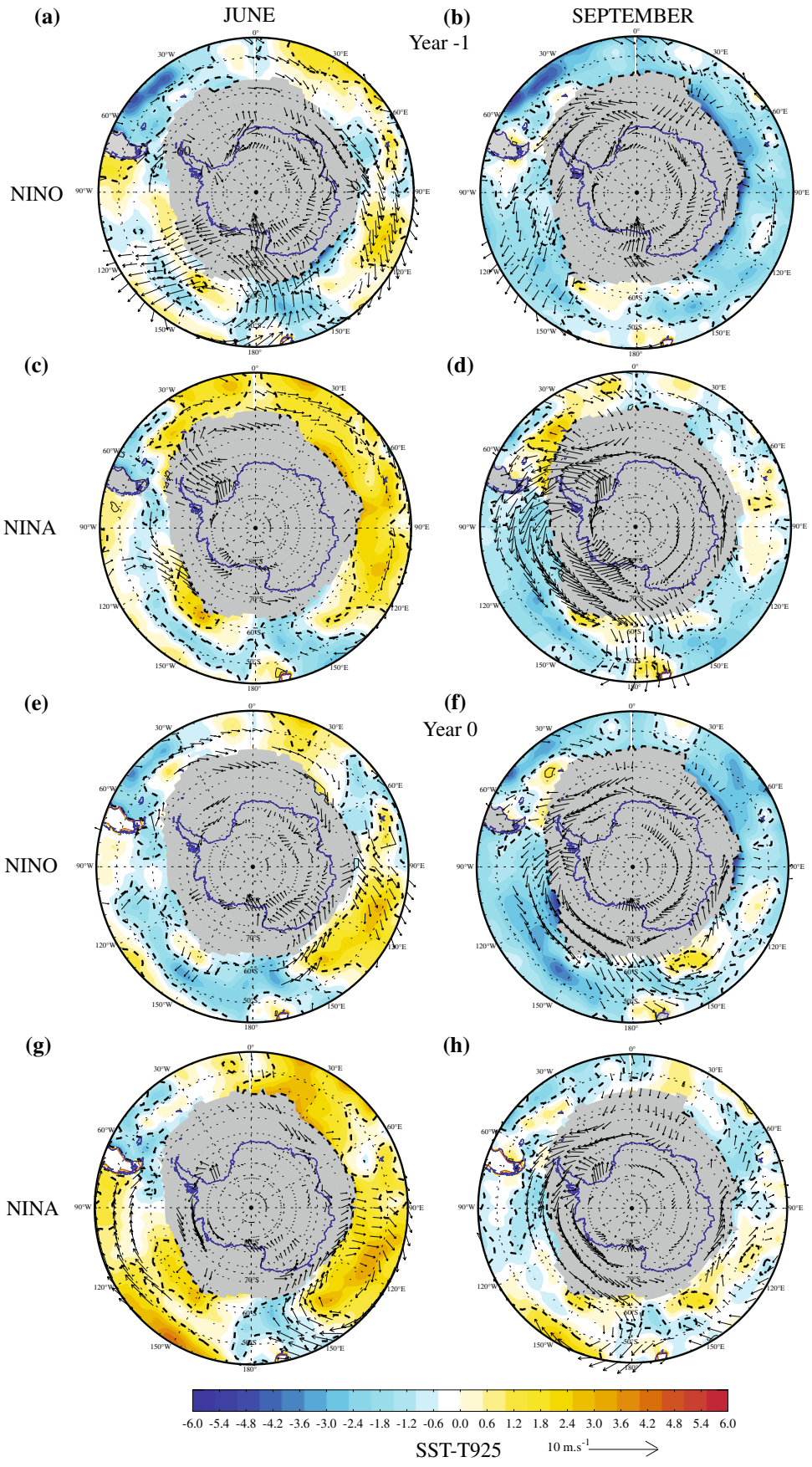

Fig. 7 Composite standardized anomalies of the difference SST-T925 and **V**925 with respect to ENSO warm (i.e., El Niño) and cold (La Niña) events for June and September of year-1 (four *panels above*) and year0 (four *panels below*). Only anomalies in **V**925 corresponding to a 90% confidence level following a phase-scrambling procedure with 999 samples are plotted (See text for more details). For (SST-T925) anomaly, the 90% confidence level is superimposed (*dashed line*). *Gray areas* correspond to grid points where at least one SST monthly value used to construct the composites was set to "undefined" because of land or sea ice

Bellingshausen/Amundsen seas in La Niña winter 1989 (Carleton and Song 2000), strong low-level winds having a persistent southerly component -and many mesocyclones- can be involved in this within-season reversal of the vertical temperature gradient in the lower atmosphere, in contrast to a winter (e.g., 1988) of weaker westerlies and more frequent northerly components**.** It should be noted that the progression from June to September is relatively smooth (not shown).

For warm events (Nino in year-1; Fig. 7a, b), in the area near and south of New Zealand, northerly wind anomalies are superimposed on decreased SST-T925 anomalies, comprising conditions not favorable for meso-cyclogenesis. Conversely, over the Indian Ocean from 70°E to 130°E, and in the southern Pacific Ocean and Amundsen Sea, southerly wind anomalies blowing over positive vertical temperature anomalies, are favorable for meso-cyclogenesis. This situation contrasts with El Niño events in year0 (Fig. 7e, f) for which the area southwest of New Zealand, especially in September, has associated strong southerly winds and a slight increase of the (SST-T925) index. Similarly, over the Indian Ocean, favorable anomaly conditions for mesocyclone development are restricted to the longitude range 90–120°E consistent with, for example, a reduced number of mesocyclones over the Indian Ocean in 1982, compared to 1981. Unfavorable anomaly conditions are also seen to the north of the Weddell Sea for year-1 and, to a lesser extent, for year0.

The composite fields for La Niña events also display features consistent with the mesocyclone distribution depicted in Fig. 6. In year-1, persistent northerly or northeasterly wind anomalies and reduced vertical temperature anomalies are observed over the Amundsen Sea; unfavorable for meso-cyclogenesis (Fig. 7c, d). This contrasts with the Weddell Sea, and the area south of New Zealand, where, especially in September, there is stronger southerly flow, an increased SST-T925 temperature and low T500 (not shown). For La Niña in year0 (Fig. 7g, h), larger SST-T925 over a large part of the southern oceans, when associated with anomalous southerly flow and low temperatures at the 500 hPa level (Fig. 8), gives rise to more mesocyclones. This is the case, for example, between 80° and 120°E in June, and over sea-ice areas of the western Ross Sea and further north. However, to the west of 180°E, the anomaly pattern indicates northerly flow combined with reduced SST-T925, which contributes to a dearth of mesocyclones there, in agreement with what is observed for 1989 (Fig. 6).

The above-described mesocyclone-favorable and unfavorable conditions generally are amplified by anomalies of the mid-tropospheric temperature (T500) and the sea ice conditions associated with ENSO. As an example, T500 anomaly composites for June in year-1 of El Niño (Fig. 8a), show unfavorable conditions in terms of SST-T925 and **V**925 to the south of New Zealand and in the South Atlantic Ocean, and north of the Weddell Sea, to be associated with higher T500, which inhibits mesocyclone formation. In contrast, lower T500 centered at about 120°E in El Niño year-1 and year0 (Fig. 8b), coincides with more mesocyclones. The colder air in the mid-troposphere associated with La Niña events centered at about 120°E, 120°W and 30°W in year-1 (Fig. 8c), and 30°E in year0 (Fig. 8d), favors meso-cyclogenesis. In terms of sea ice conditions, differences in the ice edge (defined as the 90% concentration limit) between June and September for Niño and Niña years (Fig. 9) are shown only for year0 because they exhibit rather similar structures for year-1. It is interesting that the areas where the ice limit is stagnant or located even more poleward in September than in June also accompany minima in mesocyclone frequency (e.g., for Niña events, the area between 150°E and 180° and the west of the Weddell Sea in year0; the area south of New Zealand for Niño in year-1, not shown). Conversely, areas where the ice limit is located much further northward in September than in June generally correspond to many mesocyclones.

3.3.2 Trans-Polar Index and SAM

As already observed for ENSO and in relationship with the SAO, composite anomaly fields of SST-T925 and **V**925 for winters characterized by highly positive and highly negative TPI index (Fig. 10), show a significant change between the early and late winter. More specifically, for positive TPI in early winter, the co-occurrence of increased SST-T925, more southwesterly flow (Fig. 10a) and lower T500 (Fig. 11a), create highly favorable conditions for meso-cyclogenesis over the Amundsen Sea and most of the South Indian Ocean. In late winter, a more favorable anomaly pattern occurs over the Weddell Sea and south Atlantic Ocean. For the TPI negative phase (Fig. 10c, d), two areas exhibit both larger SST-T925 positive differences and southerly flow: southwest of Australia at around 120°E, and around 150°W. Conversely, the area south of New Zealand, the Bellingshausen Sea and the area centered at about 60°E should see fewer mesocyclones because of the reduced SST-T925 difference, more northerly winds, a tendency for warmer air in mid-troposphere (Fig. 11c), and -for the first two areas - a stagnant sea ice limit (Fig. 12).

As expected from the correlations given in the preceding section (Table 1), the SAM composites of the same fields (Fig. 13) are qualitatively similar to the TPI composites. The SST-T925 anomalies associated with SAM generally are larger, especially where negative. On the other hand, the signature in T500 (Fig. 11b–d) is stronger for TPI than

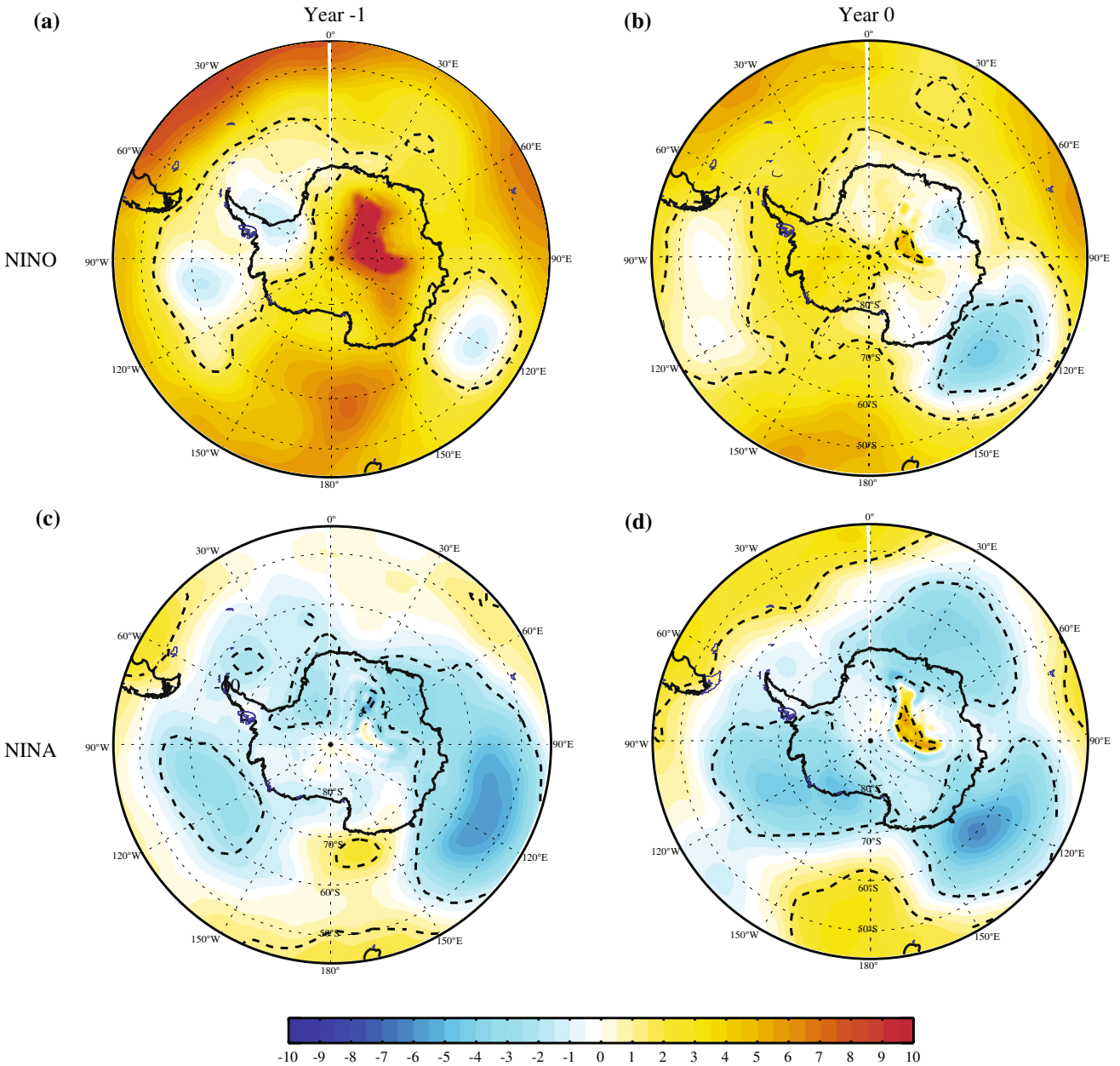

Fig. 8 Composite standardized anomalies of T500 with respect to ENSO warm (i.e., El Niño) and cold (La Niña) events for June of year-1 and year0

SAM. Additional differences between TPI and SAM composites are discussed in the last sub-section.

3.4 Links to synoptic weatther

The map patterns of reanalysis variables (composites, case winters) bridge the end spatial scales represented by mesocyclones and teleconnections, by depicting the synoptic context. Thus, areas of southerly flow, positive SST-T925, cold advection, upwelling of cold water and extensive sea ice that are favorable for meso-cyclogenesis, typify locations in and just west of the semi-permanent troughs; areas of northerly flow, negative SST-T925, warm advection, downwelling and reduced sea ice that are less favorable for meso-cyclogenesis, occur west of high pressure ridges (e.g., Milliff et al. 1999; Yuan et al. 1999). On average for winter in the SH, semi-permanent troughs—wherein synoptic-scale (frontal) cyclones develop and move south-eastward along preferred "storm tracks"—occupy the three ocean basins (e.g., Carleton 1979; Carleton 1992; Berbery and Vera 1996). The most prominent of these troughs occurs in the central and south-east South

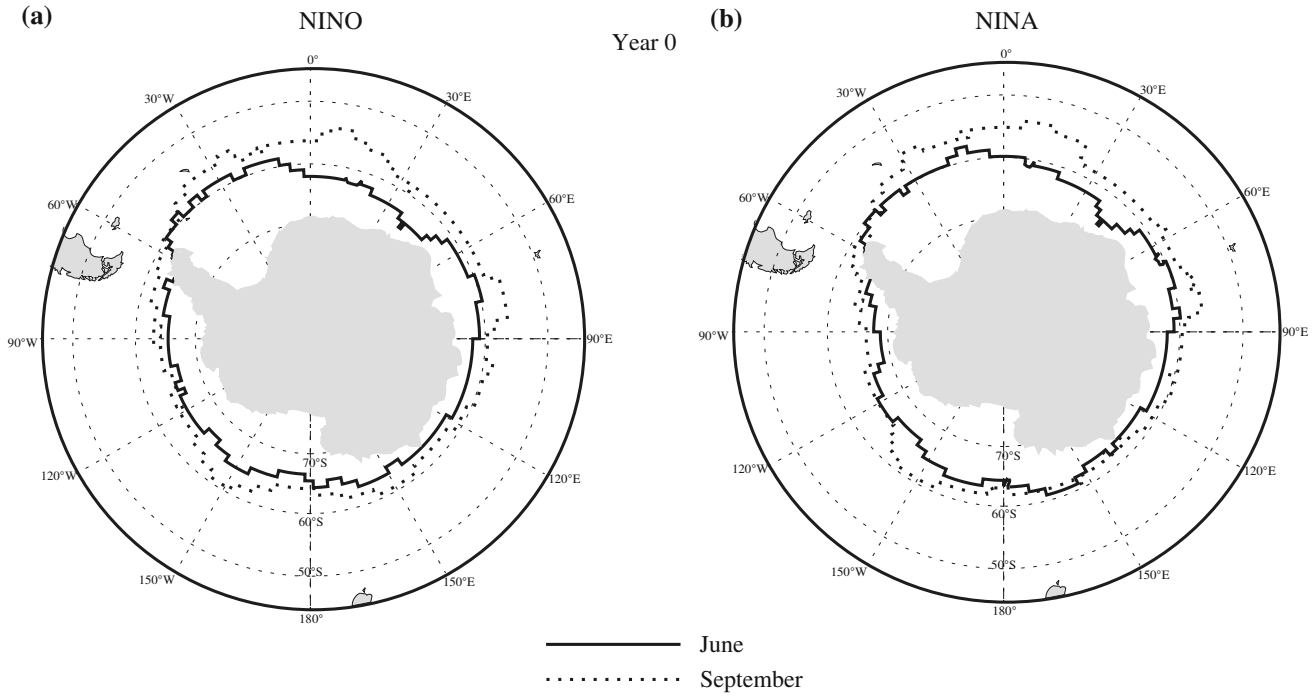

Fig. 9 Sea ice edge in June and September for composite ENSO warm and cold events for year0

Pacific: variations in the longitude location and intensity of this trough and in the associated storm tracks are strongly connected to ENSO (e.g., Carleton and Whalley 1988). Ridges are most frequent over and just downstream of the continents in winter (e.g., Sinclair 1996); that over eastern Australia and the Tasman Sea undergoes strong variations related to ENSO (van Loon 1984; Marques and Rao 2000). The evolution of frontal cyclones, from cyclo-genesis through maturity to cyclo-lysis, typically takes place at successively higher latitudes, with maximum frequencies occurring at around 60°S in and just north of the circumpolar trough (e.g., Tucker 1979; Turner et al. 1996, their Fig. 15; Simmonds and Keay 2000). Accordingly, mesocyclones occur preferentially in the cold-air advection -and enhanced convection- typical of the western and south-western sides of these systems; behind the troughs (e.g., south-west South Pacific; southern Indian Ocean). Conversely, mesocyclones are not favored in the warm advection and extensive areas of stratiform cloud east and south-east of these systems, ahead of the troughs and west of ridges (e.g., south-east South Pacific).

3.5 Meso-cyclogenesis potential for teleconnection phases

Having determined the composite associations between winter mesocyclone distributions and several key atmospheric and oceanic variables (Sect. 3.1), and between the latter sets of reanalyses and large-scale SH teleconnection patterns (Sect. 3.3), we can identify those spatial areas favorable, and also unfavorable, for meso-cyclogenesis; the *meso-cyclogenesis potential,* which refers to activity relative to background levels. For each teleconnection phase, the likeliest areas of enhanced meso-cyclogenesis, relative to winter background frequencies, are those where multiple mesocyclone-favorable conditions characteristic of each teleconnection overlap. Similarly, those areas most likely to see decreased winter meso-cyclogenesis compared to the climatology are depicted as the spatial coincidence of multiple unfavorable conditions. Figure 14a–h shows maps of enhanced meso-cyclogenesis potential for ENSO (El Niño, La Niña), SAM and TPI, based upon the early winter (June) composite favorable conditions identified earlier; i.e., negative anomalies of T500; positive anomalies of (SST-T925); anomalies of **V**925 having a southerly component; and proximity to the sea-ice edge, given as a location within ±2.5° latitude (this last point related to low level baroclinicity that occurs when cold dry air blows off the ice edge towards lower latitudes, CF93). Four classes of relative (i.e., categorical) probability of enhanced meso-cyclogenesis are identified, as follows: (1) Maximum Probability: the co-occurrence of all 4 favorable conditions; (2) High Probability: all but one favorable condition is present; (3) Moderate Probability: any two favorable conditions co-occur; (4) Increased Probability: any one favorable condition is present, or two favorable conditions co-occur but with a meso-cyclogenesis unfavorable condition also present (e.g., positive T500 anomalies).

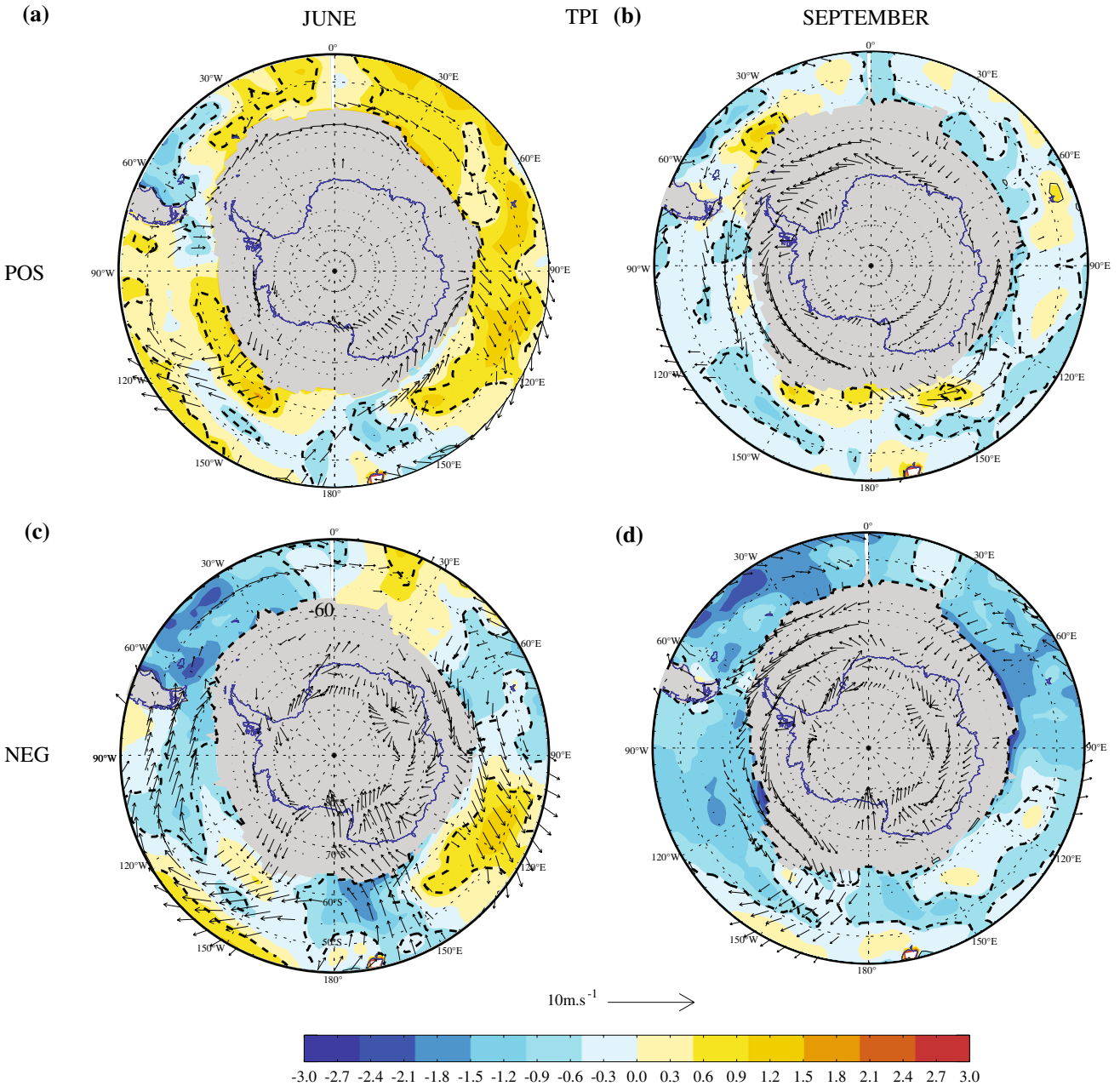

Fig. 10 Same as Fig. 7 but for TPI

Although refinement of these four probability classes to include a greater number of classes, or to weight the importance of each favorable condition, probably is desirable, such an undertaking would involve explicit consideration of the regional dependence of each factor in meso-cyclogenesis; for example, emphasizing the katabatic winds in the Ross Sea sector versus an upper cold pool of air in the Amundsen/Bellingshausen seas (cf. Fitch and Carleton 1992; CF93). Also, over ice shelves or sea ice covered areas, the maximum probability cannot be reached because the SST-T925 criterion does not apply. Notwithstanding, the present maps (Fig. 14) are useful for depicting the general hemispheric-scale spatial variations of meso-cyclogenesis potential at the start of winter according to teleconnection phases. Even given that the two kinds of maps show somewhat different quantities—meso-cyclogenesis potential areas mostly are located upstream of where meso-cyclones spin up, move to, and dissipate—they compare quite well for case winter months or seasons (below).

Examination of Fig. 14 shows that the largest (smallest) variations in meso-cyclogenesis potential across

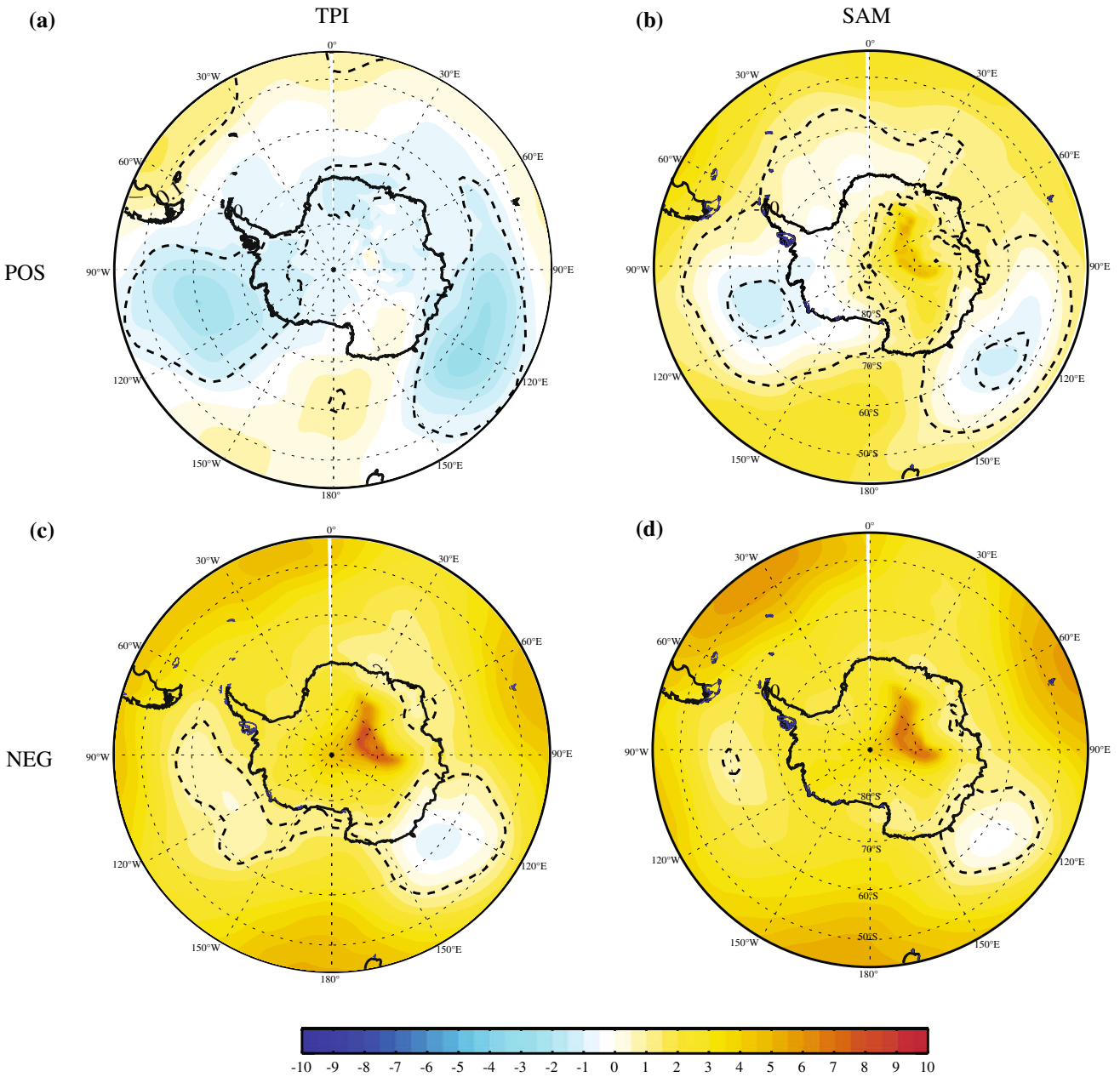

Fig. 11 Composite standardized anomalies of T500 with respect to TPI and SAM for June

teleconnections occur in the South Pacific (South Indian Ocean and waters south of Australia), and are dominated by ENSO. Meso-cyclogenesis potential in the early winter of El Niño year0 (Fig. 14a) shows large areas of maximum and also high probability in the eastern hemisphere, but a relative dearth of favorable conditions in the western hemisphere, especially the South Pacific. The strong activity suggested for the southern and south-eastern Indian Ocean compares well with the distribution of meso-cyclones identified for the El Niño winter 1992 (Carleton and Song 1997; their Figs. 2 and 3) and, to an extent, the extreme event of 1982 (Fig. 2c). The lack of activity in the South Pacific also is similar to that identified for the 1988 winter (Fig. 3a). A comparison of Fig. 14a, with that for El Niño year-1 (Fig. 14b) shows much greater meso-cyclogenesis potential in the South Pacific in the early winter before an El Niño. The latter is consistent both with the pattern shown for winter 1981 (Fig. 2b), and with previous studies of the change in atmospheric circulation (e.g., as represented in sea level pressure) over this sector in the lead-up to an El Niño event (van Loon and Shea 1985). Additionally, Fig. 14b, suggests an areal expansion of meso-cyclogenesis potential in the eastern hemisphere during an El Niño (year-1) early winter.

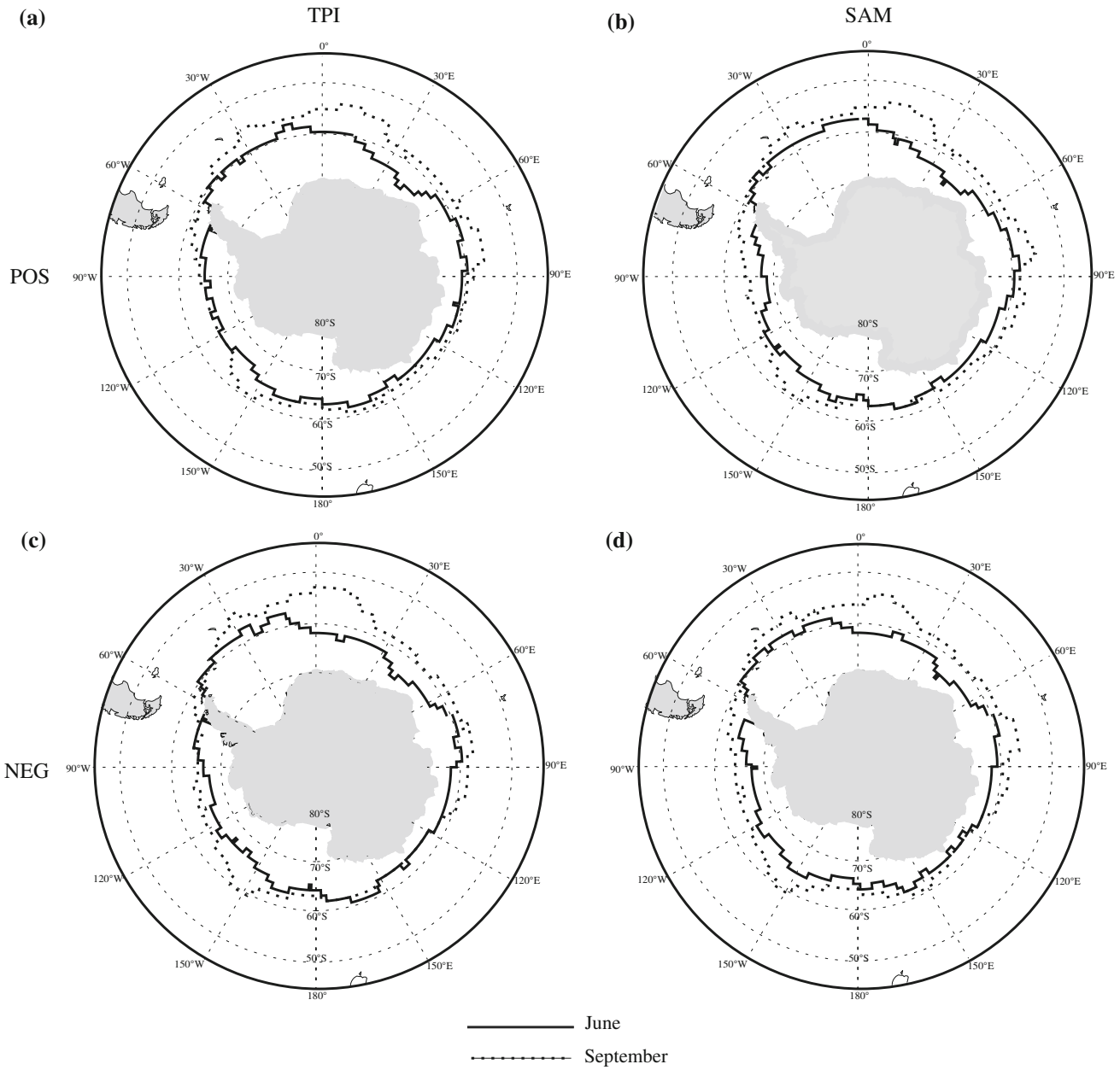

Fig. 12 Same as Fig. 9 but for TPI and SAM

Compared to El Niño (year0), the meso-cyclogenesis potential in La Niña early winters (year0) is greater over most areas, especially the South Pacific (Fig. 14c). The latter compares well with the mesocyclone distributions shown for this region in winter 1989 (Fig. 3b), and further supports the general similarity between El Niño (year-1) and La Niña (year0) circulation noted in previous studies (e.g., van Loon and Shea 1985; Carleton 1988). Inspection of the La Niña (year-1) map (Fig. 14d) suggests comparable meso-cyclogenesis potential to La Niña (year0) in the southern Indian Ocean and South Pacific, but with strong increases for the Atlantic Ocean and decreases around 180° longitude.

For SAM Positive early winters (Fig. 14e), enhanced meso-cyclogenesis potential occurs over all areas of the Southern Ocean, except the south-west Atlantic and western South Pacific. The areas of "maximum" and "high" probabilities identified for the Bellingshausen/Amundsen Seas compare well with the summary map of winter mesocyclone tracks shown for this region and extending downstream over the Antarctic Peninsula in SAM Positive early winters (cf. Lubin et al. 2008; their Fig. 1b). In SAM Negative winters (Fig. 14f), the meso-cyclogenesis potential decreases in magnitude over wide areas relative to SAM Positive years, largely the result of extensive T500

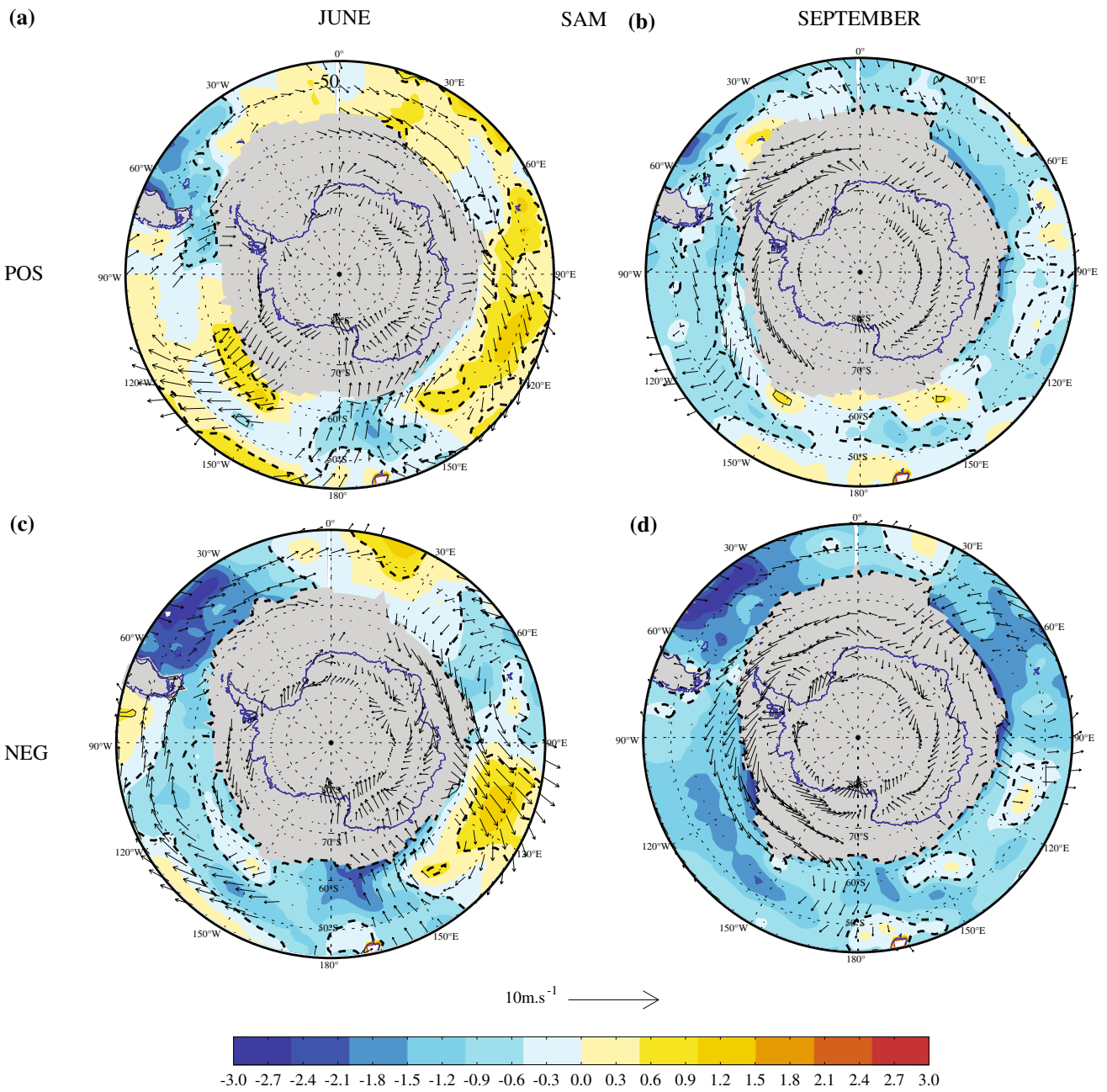

Fig. 13 Same as Fig. 7 but for SAM

positive anomalies. In the Amundsen/Bellingshausen sector, a split pattern of enhanced activity is suggested. Figure 14e, f are in fair agreement with results shown by Lubin et al. (2008, their Fig. 1a, b), who showed that there are more mesocyclones in particular in the Amundsen-Bellingshausen and the Weddell Seas under positive versus negative SAM index conditions.

Winters marked by positive extremes of the TPI (Fig. 14g) have associated two broad areas of enhanced meso-cyclogenesis potential, as follows: (1) the southern Indian Ocean and adjacent waters south of Australia; and (2) the south-east South Pacific. Although winter 1981 was an El Niño year-1, it was also marked by a change to quite strongly positive TPI between June and September (CC90; their Table VII), and there is some correspondence between Figs. 2a, and 14g. The meso-cyclogenesis potential map for TPI Negative winters (Fig. 14h) suggests three broad areas of enhanced activity: the Weddell Sea and south-east Atlantic Ocean; the Southern Ocean south of Australia; and the central South Pacific. Figure 14h, can reasonably be compared with the map of mesocyclone locations derived for the 1978 winter (Carleton and Carpenter 1989; their

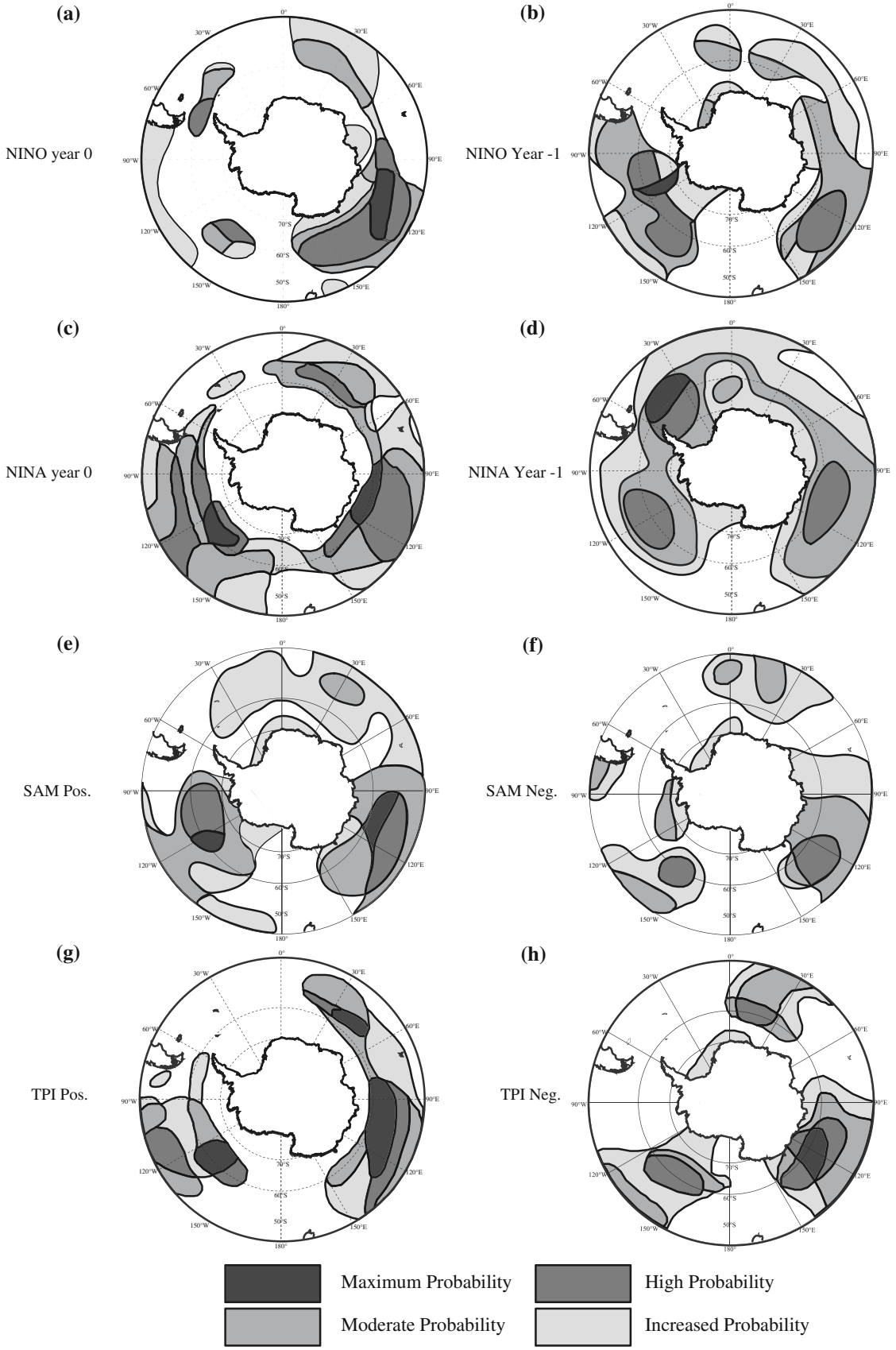

Fig. 14 Maps of enhanced meso-cyclogenesis potential (refer text) in early winter associated with large-scale teleconnections (four classes)

Fig. 7), when the TPI became strongly negative between June and September (CC90; their Table VII); in particular, the South Atlantic sector and region south of Australia.

In identifying and delineating those areas of enhanced meso-cyclogenesis potential in winter according to teleconnection phase (Fig. 14a–h), it is also instructive to determine those areas least likely to experience such activity; that is, where winter meso-cyclogenesis would be expected to decrease the most relative to background levels (here, two classes: "Least Favorable"; "Not Favorable"; denoting the spatial coincidence of all or all-but-one, respectively, of the following conditions: positive anomalies of T500; negative values of (SST-T925); anomalies of **V**925 having a predominantly northerly component; and location either remote from the sea-ice–ocean margin or where the ice edge is located at higher latitudes). Although the areas of suppressed meso-cyclogenesis potential (Fig. 15a–h) occupy unshaded areas on the maps of enhanced potential (Fig. 14a–h), they are not necessarily mirror images of those maps: areas of high and low potential can be located either close to one another (e.g., in the south-west Pacific) or some distance away. In general, the meso-cyclogenesis potential accompanying teleconnection patterns is suppressed in middle-latitude regions where northerly low-level wind anomalies (i.e., **V**925) blow over negatives differences in (SST-T925) west of ridges/east of troughs. Particularly in longitudes of New Zealand, the meridionally-oriented areas of suppressed meso-cyclogenesis potential likely manifest frequent blocking ridges (e.g., in El Niño year(-1); Fig.15c). Moreover, the area just east of southern South America is indicated as unfavorable for meso-cyclogenesis across all teleconnection phases considered here. There is support for both these unfavored regions in the mesocyclone density maps for case winters (e.g., Fig. 2 a, b). Also, the teleconnection phase suggested as having the smallest area of unfavorable conditions in longitudes of New Zealand—the El Niño year(0) (Fig. 15a)—is distinguished by having large numbers of mesocyclones in this region during winter 1982 (Fig. 2c), contrasted with El Niño(year-1).

4 Summary and conclusions

To improve both the short-term (i.e., weather) and climate-scale predictions of cold-air mesocyclone "watch areas" (e.g., enhanced meso-cyclogenesis potential) over the Southern Ocean, we have identified the associated composite atmospheric and oceanic large-scale environments on monthly and multi-monthly time scales for the winter season. Determination of mesocyclone-favorable and unfavorable conditions involves comparisons with previously developed (from satellite image interpretation) inventories of mesocyclones for several winters marked by opposite phases of the ENSO (El Niño, La Niña) teleconnection. They also rely on the long-term high-resolution reanalysis ERA-40, shown to be reliable over high southern latitudes for the period beginning 1979. These investigations show that mesocyclone frequencies increase when and where the SST-T925 difference increases, overlain by south to southwesterly low-level winds (i.e., strong upward fluxes of heat and moisture occur to the west and southwest of troughs and frontal cyclones). Additional favorable conditions for mesocyclones include low temperatures at 500 hPa, typically accompanied by greater sea ice extent in those longitudes. Conversely, unfavorable conditions for mesocyclone development involve negative or only weakly positive SST-T925; low-level winds with northerly components (i.e., stable lower atmosphere); warm air at 500 hPa; and reduced sea ice (i.e., downward fluxes of heat located east of frontal cyclones and west of high pressure ridges). It must be added that local factors such as katabatic winds also play a role in the development of cold-air mesoyclones, and have not been considered here. Because such an assessment should be made at a regional scale, it will be the subject of a further study.

The second objective of the study was to apply the relationships identified for case study years to the climatic context, through statistical analysis of the interrelationships between broad-scale indices of the SH circulation for the period of interest (1979–2001), and also for the preceding period (1957–1978), and to determine the associations of mesocyclone-favored reanalysis variables with the three large-scale SH teleconnection patterns (ENSO, SAM, TPI). For the period 1979–2001, these teleconnections are uncorrelated during winter months, with the exception of SAM and TPI, especially in late winter. Thus, we have inferred the preferred spatial locations for mesocyclones according to opposite phases of the teleconnections, and compared similar months of early winter (June) or late winter (September) because of the influence of the SAO.

Utilizing the composite anomaly fields of mesocyclone-favorable, and also unfavorable, conditions, we derive spatial patterns of enhanced and suppressed meso-cyclogenesis potential associated with the teleconnections. For the hemisphere as a whole, the meso-cyclogenesis potential is dominated by ENSO; secondarily by SAM, although there are some strong regional-scale variations associated with the latter. Generally good agreement between the maps of meso-cyclogenesis potential and mesocyclone distributions in case winters occurs despite the two map types representing somewhat different quantities. The method to generate meso-cyclogenesis potential maps should next be applied to regional-scale teleconnection patterns, such as PSA and ADP, with modifications that consider spatial differences in the relative importance of

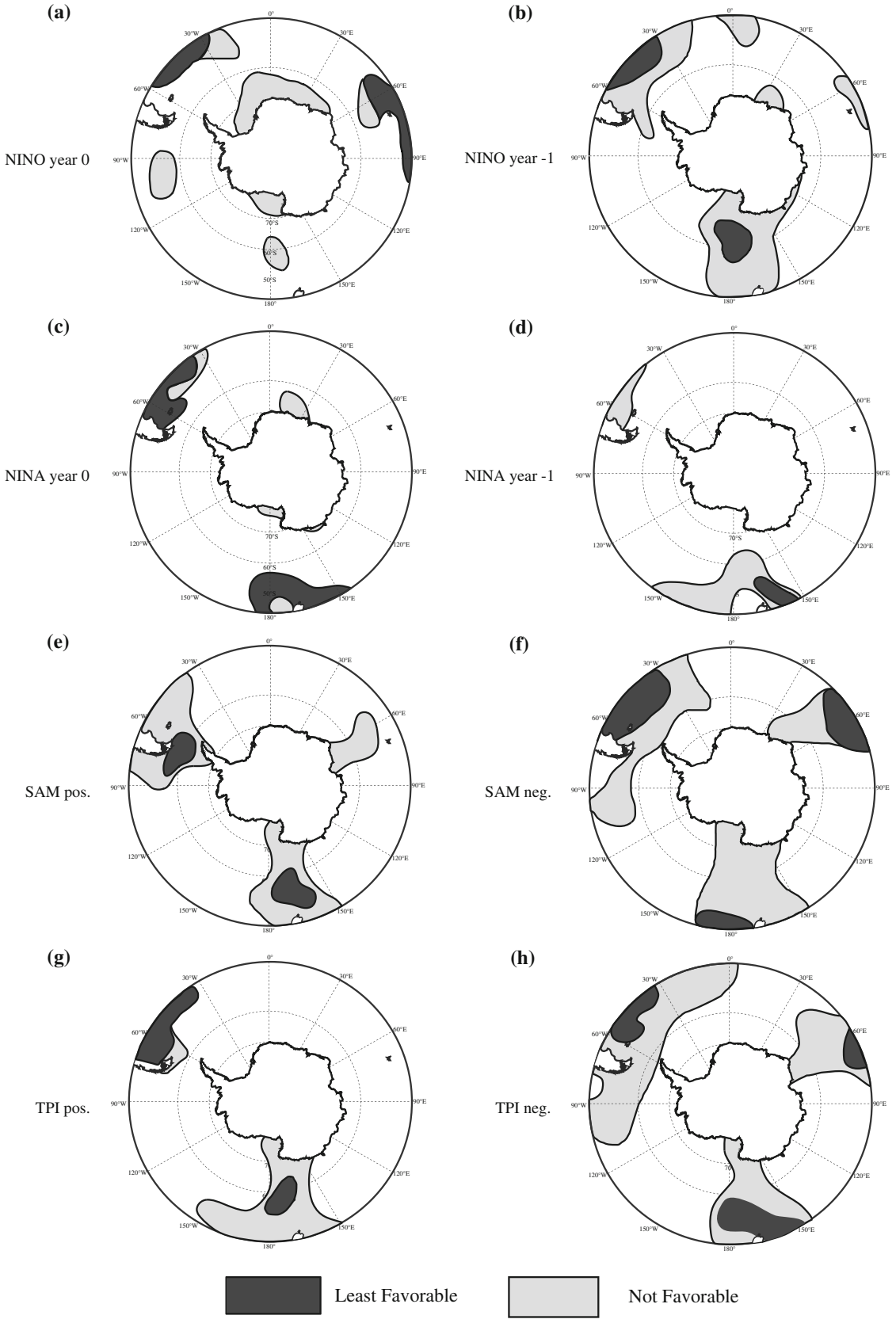

Fig. 15 Maps of suppressed meso-cyclogenesis potential (refer text) for early winter associated with large-scale teleconnections (2 end probability classes)

mesocyclone physical processes (e.g., katabatic winds versus cold pool aloft). The validity of those associations should be tested against mesocyclone distributions determined for additional case months and seasons utilizing satellite-image analysis.

In terms of ENSO, the results both confirm and extend observations previously made on case study years characterized by contrasting climate and circulation conditions: they show unfavorable conditions for meso-cyclogenesis near and south of New Zealand, and over the south-western Atlantic Ocean during La Niña (year0) events, and generally the reverse for El Niño (year0) events. Conditions are more favorable in the Amundsen Sea during La Niña than during El Niño events. These favorable and unfavorable anomaly patterns as depicted by SST-T925 differences and **V**925, are generally amplified by the mid-tropospheric (500 hPa) temperature and sea ice conditions associated with ENSO. Our results also indicate significant changes in the locations of meso-cyclogenesis from year-1 to year0.

With regard to SAM, to the knowledge of the authors and despite a large number of studies aimed at assessing this teleconnection's impact on surface, oceanic, and atmospheric fields over high southern latitudes (e.g., Yuan and Martinson 2000; Hall and Visbeck 2002; Genthon et al. 2003; Lefebvre et al. 2004, and references herein), there has been no attempt to characterize the SAM associations with mesocyclone developments on a hemispheric scale. The study by Lubin et al. (2008) considers only the south-east Pacific through south-west Atlantic region centered on the Antarctic Peninsula. Our analysis indicates that a positive SAM or TPI index favors cold-air mesoyclogenesis practically everywhere over the southern oceans in winter with the exception of the eastern Bellingshausen Sea and between approximately 180°–160°E, the latter being particularly a preferred sector for blocking ridges. A negative SAM or TPI phase inhibits meso-cyclogenesis south of New Zealand, and also in the Bellingshausen Sea and the area centered at about 60°E.

The associations identified above between large-scale circulation and mesocyclone regimes suggest some predictive skill to the general areas of enhanced and also suppressed mesocyclone activity during winter, assuming a reasonably accurate forecast of teleconnection phase(s). Seasonally, this is easier for ENSO owing to the stronger month-to-month persistence, whereas for the extratropical indices (TPI, SAM) the skill may be limited to monthly time scales (e.g., Carleton 1989). In the longer context of contemporary climate warming, the projected continued strengthening of the SAM; sea ice retreat; changes in the SAO (e.g., Bracegirdle et al. 2008); together with changes in frequencies of Antarctic cold-air outbreaks (Kolstad and Bracegirdle 2008 for the Northern Hemisphere); likely will impact meso-cyclogenesis via changes to the ocean-ice–atmosphere interaction. Finally, this study supports the value of analyzing older datasets (the mesocyclone spatial inventories) in the context of newly available reanalysis and other data.

Acknowledgments The support of U.S. National Science Foundation grants SES-8603470 and DPP-8816912 to Andrew M. Carleton is gratefully acknowledged. ERA-40 data have been obtained from the ECMWF Data Server. Sebastien Masson provided graphical software (SAXO) for plotting the results.

References

Berbery EH, Vera CS (1996) Characteristics of the southern hemisphere winter storm track with filtered and unfiltered data. J Atmos Sci 53:468–481

Bracegirdle TJ, Connolley WM, Turner J (2008) Antarctic climate change over the twenty-first century. J Geophys Res 113:D03103. doi:10.1029/2007JD008933

Bromwich DH (1991) Mesoscale cyclogenesis over the south-western Ross Sea linked to strong katabatic winds. Mon Weather Rev 119:1736–1752

Bromwich DH, Fogt RT (2004) Strong trends in the skill of the ERA-40 and NCEP-NCAR reanalyses in the high and middle latitudes of the southern hemsiphere, 1958–2001. J Clim 17:4603–4619

Bromwich DH, Carrasco JF, Turner J (1996) A downward developing mesoscale cyclone over the ross ice shelf during winter. Global Atmos Ocean Syst 4:125–147

Bromwich DH, Rogers AN, Kållberg P, Cullather RI, White JWC, Kreutz KJ (2000) ECMWF analyses and reanalyses depiction of ENSO signal in Antarctic precipitation. J Clim 13:1406–1420

Budd WF (1975) Antarctic sea-ice variations from satellite sensing in relation to climate. J Glaciol 15:417–427

Businger S (1985) The synoptic climatology of polar-low outbreaks. Tellus 37A:419–432

Businger S (1987) The synoptic climatology of polar-low outbreaks over the Gulf of Alaska and the Bering Sea. Tellus 39A:307–325

Businger S, Reed RJ (1989) Cyclogenesis in cold air masses. Weather Forecast 2:133–156

Carleton AM (1979) A synoptic climatology of satellite-derived extratropical cyclone activity for the southern hemisphere winter. Arch Met Geophys Bioklim B27:265–279

Carleton AM (1981) Monthly variability of satellite-derived extratropical cyclone activity for the southern hemisphere winter. J Climatol 1:21–38

Carleton AM (1985) Satellite climatological aspects of the "polar low" and "instant occlusion". Tellus 37A:433–450

Carleton AM (1987) Satellite-derived attributes of cloud vortex systems and their application to climate studies. Remote Sens Environ 16:2457–2485

Carleton AM (1988) Sea ice—atmosphere signal of the Southern Oscillation in the Weddell Sea, Antarctica. J Clim 1:379–388

Carleton AM (1989) Antarctic sea-ice relationships with indices of the atmospheric circulation of the southern hemisphere. Clim Dyn 3:207–220

Carleton AM (1992) Synoptic interactions between Antarctica and lower latitudes. Aust Meteorol Mag 40:129–147

Carleton AM (1995) On the interpretation and classification of mesoscale cyclones from satellite infrared imagery. Int Jour Remote Sens 16:2457–2485

Carleton AM (2003) Atmospheric teleconnections involving the Southern Ocean. J Geophys Res 108:8080. doi:10.1029/2000JC000379

Carleton AM, Carpenter DA (1989) Intermediate-scale sea ice–atmosphere interactions over high southern latitudes in winter. GeoJournal 18:87–101
Carleton AM, Carpenter D (1990) Satellite climatology of "polar lows" and broadscale climatic associations for the southern hemisphere. Int J Climatol 10:219–246
Carleton AM, Fitch M (1993) Synoptic aspects of Antarctic mesocyclones. J Geophys Res 98:12997–13018
Carleton AM, Song Y (1997) Synoptic climatology and intrahemispheric associations of cold air mesocyclones in the Australasian sector. J Geophys Res 102:13873–13887
Carleton AM, Song Y (2000) Satellite passive sensing of the marine atmosphere. Prof Geogr 52:289–306
Carleton AM, Whalley D (1988) Eddy transport of sensible heat and the life history of synoptic systems: A statistical analysis for the southern hemisphere winter. Meteor Atmos Phys 38:140–152
Carleton AM, McMurdie L, Katsaros KB, Zhao H, Mognard N, Claud C (1995) Satellite-derived features and associated atmospheric environments of Southern Ocean mesocyclone events. Global Atmos Ocean Syst 3:209–248
Carrasco JF, Bromwich DH (1994) A survey of mesoscale cyclonic activity near McMurdo Station, Antarctica. Ant J of the US 29:298–301
Carrasco JF, Bromwich DH, Liu Z (1997) Mesoscale cyclone activity over Antarctica during 1991. 2. Near the Antarctic Peninsula. J Geophys Res 102:13939–13954
Carrasco JF, Bromwich DH, Monaghan AJ (2003) Distribution and characteristics of mesoscale cyclones in the Antarctic: Ross Sea eastward to the Weddell Sea. Mon Weather Rev 131:289–301
Cavalieri DJ, Parkinson CL (1981) Large-scale variations in observed Antarctic sea ice extent and associated atmospheric circulation. Mon Weather Rev 109:2323–2336
Cavalieri D, Parkinson C, Gloersen P, Zwally HJ (1996, updated 2006) Sea ice concentrations from Nimbus-7 SMMR and DMSP SSM/I passive microwave data. Boulder, Colorado USA: National Snow and Ice Data Center. Digital media
Claud C, Katsaros KB, Mognard NM, Scott NA (1996) Comparative satellite study of mesoscale disturbances in polar regions. Global Atmos Ocean Syst 4:233–273
Claud C, Heinemann G, Raustein E, McMurdie L (2004) Polar low « le cygne » : Satellite observations and numerical simulations. Q J R Meteorol Soc 130:1075–1102
Claud C, Duchiron B, Terray P (2007) Associations between large-scale atmospheric circulation and polar low developments over the North Atlantic during winter. J Geophys Res 112:D12101. doi:10.1029/2006JD008251
Cullather RI, Bromwich DH, van Woert ML (1996) Interannual variability in Antarctic precipitation related to El Nino Southern Oscillation. J Geophys Res 101:19109–19118
Davison AC, Hinkley DV (1997) Bootstrap methods and their application, Cambridge University Press, London, p 582
Emanuel KA, Rotunno R (1989) Polar lows as arctic hurricanes. Tellus 41A:1–17
Enomoto H, Ohmura A (1990) The influence of atmospheric half-yearly cycle on the sea ice extent in the Antarctic. J Geophys Res 95:9497–9511
Ese T, Kanestrom I, Pedersen K (1988) Climatology of polar lows over the Norwegian and Barents Seas. Tellus 40A:248–255
Farrara JD, Ghil M, Mechoso CR, Mo KC (1989) Empirical orthogonal functions and multiple flow regimes in the southern hemisphere winter. J Atmos Sci 46:3219–3223
Fitch M, Carleton AM (1992) Antarctic mesocyclone regimes from satellite and conventional data. Tellus 44A:180–196
Fogt RL, Bromwich DH (2006) Decadal variability of the ENSO teleconnection to the high latitude South Pacific governed by coupling with the Southern Annular Mode. J Clim 19:979–997
Forbes GS, Lottes WD (1985) Classification of mesoscale vortices in polar airstreams and the influence of the large-scale environment on their evolution. Tellus 37A:132–155
Genthon C, Cosme E (2003) Intermittent signature of ENSO in west-Antarctic precipitation. Gephys Res Lett 30:2081. doi:10.1029/2003GL019280
Genthon C, Krinner G, Sacchettini M (2003) Interannual Antarctic tropospheric circulation and precipitation variability. Clim Dyn 21:289–307. doi:10.1007/s00382-003-0329-1
Gong D, Wang S (1999) Definiton of Antarctic Oscillation index. Gephys Res Lett 26:459–462
Guymer LB, LeMarshall JF (1980) Impact of FGGE buoy data on southern hemisphere analyses. Aust Meteorol Mag 28:19–42
Hall A, Visbeck M (2002) Synchronous variability in the southern hemisphere atmosphere, sea ice and ocean resulting from the Annular Mode. J Clim 15:3043–3057
Harangozo SA (1997) Atmospheric meridional circulation impacts on contrasting winter sea ice extent in two years in the Pacific sector of the Southern Ocean. Tellus 49:388–400
Harold JM, Bigg GR, Turner J (1999) Mesocyclone activity over the Northeast Atlantic. Part 2: an investigation of causal mechanisms. Int J Climatol 19:1283–1299
Harrold TW, Browning KA (1969) The polar low as a baroclinic disturbance. Q J R Meteorol Soc 95:710–723
Heinemann G (1990) Mesoscale vortices in the Weddell Sea region (Antarctica). Mon Weather Rev 118:779–793
Heinemann G, Claud C (1997) Report of a workshop on "Theoretical and observational studies of polar lows" of the European Geophysical Society Polar Lows Working Group. Bull Am Met Soc 78:2643–2658
Hewson TD, Craig GC, Claud C (2000) Evolution and mesoscale structure of a polar low outbreak. Q J R Meteorol Soc 126(A):1031–1063
Karoly DJ (1990) The role of transient eddies in low-frequency zonal variations of the southern hemisphere circulation. Tellus 42A:41–50
Kidson JW (1999) Principal modes of southern hemisphere low-frequency variability obtained from NCEP-NCAR reanalyses. J Clim 12:2808–2830
Kolstad EW, Bracegirdle TJ (2008) Marine cold-air outbreaks in the future: an assessment of IPCC AR4 model results for the Northern Hemisphere. Clim Dyn 30:871–885. doi:10.1007/s00382-007-0331-0
Lefebvre W, Goosse H (2008) An analysis of the atmospheric processes driving the large-scale winter sea ice variability in the Southern Ocean. J Geophys Res 113:C02004. doi:10.1029/2006JC004032
Lefebvre W, Goosse H, Timmermann R, Fichefet T (2004) Influence of the Southern Annular Mode on the sea ice-ocean system. J Geophys Res 109:C09005. doi:10.1029/2004JC002403
L'Heureux M, Thompson DWJ (2006) Observed Relationships between the El Nino-Southern Oscillation and the extratropical zonal-mean circulation. J Clim 19:276–287
Limpasuvan V, Hartmann DH (1999) Eddies and the Annular Modes of Climate Variability. Geophys Res Lett 26:3133–3136
Limpasuvan V, Hartmann DH (2000) Wave-maintained annular modes of climate variability. J Clim 13:4414–4429
Lubin D, Wittenmyer RA, Bromwich DH, Marshall GJ (2008) Antarctic Peninsula mesoscale cyclone variability and climatic impacts influenced by the SAM. Geophys Res Lett 35:L02808. doi:10.1029/2007GL032170
Lyons SW (1983) Characteristics of intense Antarctic depressions near the Drake Passage, In: Preprint vol., First International Conf. on southern hemisphere meteorology, San Jose dos Campos, Brazil, 31 July–6 August 1983. Am Meteor Soc, Boston, MA, pp 238–240

Mansfield DA (1974) Polar lows: the development of baroclinic disturbances in cold air outbreaks. Q J R Meteorol Soc 100:541–554

Marques RFC, Rao VB (2000) Interannual variations of blocking in the southern hemisphere and their energetics. J Geophys Res 105:4625–4636

McMurdie LA, Claud C, Atakturk S (1997) Satellite-derived characteristics of Spiral and Comma-shaped southern hemisphere mesocyclones. J Geophys Res 102:13889–13905

Milliff RF, Hoar TJ, van Loon H (1999) Quasi-stationary wave variability in NSCAT winds. J Geophys Res 104:11425–11435

Mills JM, Walsh JE (1988) A winter mesocyclone over the Midwestern United States. Weather Forecast 3:230–242

Mo KC, Ghil M (1987) Statistics and dynamics of persistent anomalies. J Atmos Sci 44:877–901

Moore GW, Reader MC, York J, Sathiyamoorthy S (1996) Polar lows in the Labrador Sea - a case study. Tellus 48A:17–40

Ninomiya K (1989) Polar/comma cloud lows over the Japan Sea and the northwestern Pacific in winter. J Met Soc Jap 67:83–97

Pittock AB (1980) Patterns of climatic variations In Argentina and Chile-1. Precipitation, 1931–60. Mon Weather Rev 108:1347–1361

Pittock AB (1984) On the reality, stability and usefulness of southern hemisphere teleconnections. Aust Meteorol Mag 32:75–82

Rasmussen EA (1979) The polar low as an extratropical CISK disturbance. Q J R Meteorol Soc 105:531–549

Rasmussen EA (1981) An investigation of a polar low with a spiral cloud structure. J Atmos Sci 38:1785–1792

Rasmussen EA, Turner J (2003) Polar lows: mesoscale weather systems in the polar regions. Cambridge University Press, London, p 612

Rasmussen EA, Pedersen TS, Pedersen LT, Turner J (1992) Polar lows and arctic instability lows in the Bear Island region. Tellus 44A:133–154

Rasmussen EA, Claud C, Purdom JF (1996) Labrador Sea polar lows. Global Atmos Ocean Syst 4:275–333

Rasmussen EA, Turner J, Twitchell PF (1993) Report of a workshop on applications of new forms of satellite data in polar low research. Bull Am Meteorol Soc 74:1057–1073

Reed (1979) Cyclogenesis in polar airstreams. Mon Weather Rev 107:38–52

Renwick JA (2004) Trends in the southern hemisphere polar vortex in NCEP and ECMWF reanalyses. Geophys Res Lett 31:L07209. doi:10.1020/2003GL019302

Rocky CC, Braaten DA (1995) Characterization of polar cyclonic activity and relationship to observed snowfall events at McMurdo Station, Antarctica, In: Proceedings of the 4th conference on polar meteorol and oceanog. 15–20 Jan 1995. Dallas, Texas. AMS, Boston. pp 244–245

Rogers JC, van Loon H (1982) Spatial variability of sea level pressure and 500 mb height anomalies over the southern hemisphere. Mon Weather Rev 110:1375–1392

Simmonds I, Keay K (2000) Mean southern hemisphere extratropical cyclone behavior in the 40-year NCEP-NCAR reanalysis. J Clim 13:873–885

Simmons AJ, Gibson JK (2000) The ERA-40 Project Plan, ERA-40 Project Rep. Ser., 2000, 1. ECMWF, Reading, p 63

Sinclair MR (1996) A climatology of anticyclones and blocking for the southern hemisphere. Mon Weather Rev 124:245–263

Sinclair MR, Cong X (1992) Polar air stream cyclogenesis in the Australasian region: a composite study using ECMWF analyses. Mon Weather Rev 120:1950–1972

Smith SR, Stearns CR (1993) Antarctic pressure and temperature anomalies surrounding the minimum in the Southern Oscillation index. J Geophys Res 98:13071–13083

Smith TS, Reynolds RW (2003) Extended reconstruction of global sea surface temperatures based on COADS data (1854–1997). J Clim 16:1495–1510

Smith TS, Reynolds RW (2004) Improved Extended Reconstruction of SST (1854–1997). J Clim 17:2466–2477

Sterl A (2004) On the (in)homogeneity of reanalysis products. J Clim 17:3866–3873

Song Y, Carleton AM (1997) Climatological "models" of cold air mesocyclones derived from SSM/I data. Geocarto International 12:79–89

Streten NA (1977) Aspects of the year-to-year variation of seasonal and monthly mean station temperature over the southern hemisphere. Mon Weather Rev 105:195–206

Streten NA (1983) Antarctic sea ice and related atmospheric circulation during FGGE. Arch Met Geophys Bioklim A32:231–246

Streten NA, Pike DJ (1980) Characteristics of the broadscale Antarctic sea ice extent and the associated atmospheric circulation 1972–1977. Arch Met Geophys Bioklim A29:279–299

Streten NA, Troup AJ (1973) A synoptic climatology of satellite-observed cloud vortices over the southern hemisphere. Q J R Meteorol Soc 99:56–72

Thomas ER, Marshall GJ, McConnell JR (2008) A doubling in snow accumulation in the western Antarctic Peninsula since 1850. Gephys Res Lett 35:L01706. doi:10.1029/2007GL032529

Thompson DWJ, Wallace JM (2000) Annular modes in the extratropical circulation. Part I: Month-to-month variability. J Clim 13:1000–1016

Tucker GB (1979) Transient synoptic systems as mechanisms for meridional transport: An observational study in the southern hemisphere. Q J R Meteorol Soc 105:657–672

Turner J (2004) Review, the El Niño-Southern Oscillation and Antarctica. Int J Climatol 24:1–31

Turner J, Thomas JP (1994) Summer-season mesoscale cyclones in the Bellingshausen-Weddell region of the Antarctic and links with the synoptic-scale environment. Int J Climatol 14:871–894

Turner J, Lachlan-Cope TA, Thomas JP (1993) A comparison of Arctic and Antarctic mesoscale vortices. J Geophys Res 98:13019–13034

Turner J, Bromwich D, Colwell S, Dixon S, Gibson T, Hart T, Heinemann G, Hutchinson H, Jacka K, Leonard S, Lieder M, Marsh L, Pendlebury S, Phillpot H, Pook M, Simmonds I (1996) The Antarctic first regional observing study of the troposphere (FROST) project. Bull Am Met Soc 77:2007–2032

van Loon H (1967) The half-yearly oscillations in middle and high southern latitudes and the coreless winter. J Atmos Sci 24:472–486

van Loon H (1980) Transfer of sensible heat by transient eddies in the atmosphere on the southern hemisphere: an appraisal of the data before and during FGGE. Mon Weather Rev 108:1774–1781

van Loon H (1984) The Southern Oscillation, part 3, associations with the trades and with the trough in the westerlies of the South Pacific Ocean. Mon Weather Rev 112:947–954

van Loon H, Rogers JC (1981) Remarks on the circulation over the southern-hemisphere in FGGE and on its relation to the phases of the Southern Oscillation. Mon Weather Rev 109:2255–2259

van Loon H, Rogers JC (1984) Interannual variations in the half-yearly cycle of pressure gradients and zonal wind at sea level on the southern hemisphere. Tellus 36A:76–86

van Loon H, Shea DJ (1985) The Southern Oscillation, part 4, The precursors south of 15°S to the extremes of the Oscillation. Mon Weather Rev 113:2063–2074

Weatherly JW, Walsh JE, Zwally HJ (1991) Antarctic sea ice variations and seasonal air temperature relationships. J Geophys Res 96:15119–15130

Yarnal B, Henderson KG (1989a) A climatology of polar low cyclogenetic regions over the North Pacific Ocean. J Clim 2:1476–1491

Yarnal B, Henderson KG (1989b) A satellite-derived climatology of polar-low evolution in the North Pacific. Int J Climatol 9:551–566

Yuan X, Martinson DG (2000) Antarctic sea ice extent variability and its global connectivity. J Clim 13:1697–1717

Yuan X, Martinson DG (2001) The Antarctic Dipole and its predictability. Geophys Res Lett 28:3609–3612

Yuan X, Martinson DG, Liu WT (1999) Effect of air-sea-ice interaction on winter 1996 southern ocean subpolar storm distribution. J Geophys Res 104:1991–2007

Zwally HJ, Parkinson CL, Carsey FD, Gloersen P, Campbell WJ, Ramseier RO (1979) Seasonal variation of total Antarctic sea ice area, 1973–75. Antarct J US 14:102–103